HighResClimNevada: a high-resolution climatological dataset for a high-altitude region in southern Spain (Sierra Nevada)

Matilde García-Valdecasas Ojeda[1,2], Feliciano Solano-Farias[1], David Donaire-Montaño[1], Emilio Romero-Jiménez[1], Juan José Rosa-Cánovas[1,2], Yolanda Castro-Díez[1,2], Sonia R. Gámiz-Fortis[1,2], and María Jesús Esteban-Parra[1,2]

[1]Department of Applied Physics, University of Granada, Granada, 18071, Spain
[2]Atmospheric Physics Group, Andalusian Inter-University Institute for Earth System Research, Granada, 18071, Spain

Correspondence: Matilde García-Valdecasas Ojeda (mgvaldecasas@ugr.es)

Abstract. Climate datasets with very high spatiotemporal resolution are essential to assess the impacts of climate change in mountain areas, which are complex systems in which climate is very changeable. However, these regions are characterized by a lack of climatic information, and if there is any, it is usually short, sparse, or incomplete. This work presents a new series of very high resolution (1 km) gridded climate datasets for Sierra Nevada (SN), a mountain range classified as a double climate change hotspot as it is a semi-arid mountain range in the Mediterranean area that is particularly vulnerable to climate change. The database, called HighResClimNevada, consists of a set of climate data derived from a climate simulation using the Weather Research and Forecasting (WRF) model for the period from 1991–2022 and forced with the European ReAnalysis (ERA5). HighResClimNevada provides not only hourly and daily primary climate variables (i.e., near-surface temperature, precipitation, near-surface relative humidity, surface pressure, surface net radiation, and wind speed), but also bioclimatic variables, extremes indices from the Expert Team of Climate Change Detection and Indices (ETCCDI), and precipitation-hour indicators, which were postprocessed using aggregated temperature and precipitation values from primary climate variables. To evaluate the database performance, HighResClimNevada temperature and precipitation values were compared with reference datasets from different sources. In general, HighResClimNevada captures reasonably well not only the spatiotemporal variability of raw temperature, but also bioclimatic variables and extreme indices in SN. It displays comparable behavior to other climatic products but with a greater level of detail due to its higher spatial resolution. For precipitation, which is variable, more uncertain, and difficult to characterize, HighResClimNevada exhibits a higher amount of precipitation when compared to station-based, coarse satellite-based, and reanalysis-based products. However, the latter two present problems in characterizing precipitation in high mountain regions probably due to the scarcity of data in areas with high spatiotemporal variability, such as SN. The precipitation from HighResClimNevada is comparable to other climatic products like CHIRPS or CERRA-Land, which captures better the spatiotemporal variability in this region. These findings, therefore, suggest HighResClimNevada as a valuable long-term climate tool for a variety of applications, including land management, hydrometeorological research, flora and fauna phenology, and risk assessment. The reported datasets are freely available for download via the Zenodo platform (Garcia-Valdecasas Ojeda et al., 2025, https://doi.org/10.5281/zenodo.14883471).

1 Introduction

Mountain areas are particularly vulnerable to climate change due to several causes. On the one hand, these regions are characterized by extreme climatic conditions, forcing species of flora and animals to adapt to this environment. Consequently, mountains are rich in biodiversity, including endemic species. However, this fact makes these regions vulnerable as species that are high-altitude specialists may be less resilient under a changing climate. As a result, if the warming rate continues, natural ecosystems may suffer catastrophic consequences due to a decrease in biodiversity (La Sorte and Jetz, 2010) or a reduction of the habitats for many species (Parmesan, 2006). For example, the rising temperatures caused by climate change are leading to an upward migration of flora and fauna species (Parmesan, 2006). Subsequently, mountain biodiversity, particularly endemic species and those with limited dispersal capacity (Viterbi et al., 2013), is being affected by the emergence of invasive species. On the other hand, high-altitude areas play a key role in providing water resources to ecosystems and humans (Viviroli et al., 2020). These regions are, however, suffering unprecedented water stress as a result of increasing economic and demographic expansion (Beniston, 2003). This is particularly true over Mediterranean regions, where mountains serve as the main source of fresh water for downstream communities (the so-called water tower), who rely heavily on it during the late spring and summer (Polo et al., 2020). Moreover, mountains are undergoing rapid environmental change (Beniston et al., 2018; Gobiet et al., 2014), caused, among other factors, by the substantial increasing temperature trend that occurred in these areas. Many studies have reported elevation-dependent warming (EDW) due to different climate mechanisms, such as the snow–albedo feedback (Pepin et al., 2019, 2022; Rangwala and Miller, 2012). Specifically, an increasing temperature trend (around 0.13 °C per decade) has been found over European mountains such as the Alps since the 19th century (Begert and Frei, 2018), which has become more pronounced, especially after the 1980s, with a warming rate of 0.5 °C per decade (Nigrelli and Chiarle, 2023). This increased trend has also been found in southern Europe, such as the Pyrenees (0.17 °C per decade) and Sierra Nevada (0.13 °C per decade), where increasing patterns are more generalized for the minima (Esteban-Parra et al., 2022; Sigro et al., 2024). In the latter area, moreover, the drying trend in annual and winter precipitations (Esteban-Parra et al., 2022) is becoming a threat to the ecosystems that inhabit this region.

To understand the causes of many fundamental questions and applications in environmental research and ecology in a changing climate over high mountains, long and temporally consistent climate data with a high resolution in space and time is critical (Hartmann et al., 2000). This is even more relevant in high mountains, where limitations in measurement equipment or sensor maintenance make obtaining adequate climate records extremely challenging. As a result, climate information in these regions is usually short, sparse, or incomplete, and therefore, how the climate is changing in these regions remains uncertain. In this regard, regional climate models (RCMs) have proven to be useful tools as they can provide climate information regularly in space and time, allowing for the development of consistent long-term climate data in regions with difficult access. This is particularly true when working with an RCM with a high resolution ($\Delta x \leq 4\,\mathrm{km}$). At these spatial resolutions, deep convection can be explicitly resolved by the RCM instead of being parameterized, which is a reason why RCMs at kilometer-scale resolution are known as convection-permitting models (CPMs) or convection-permitting RCMs (CPRCMs). This fact implies a significantly enhanced representation of orography and land surface information. As a result, CPRCMs can better capture orographic precipitation and extreme rainfall events, as well as soil–atmosphere and cloud–radiation feedbacks and mountain snowpack (Coppola et al., 2020; Halladay et al., 2024; Lucas-Picher et al., 2024; Prein et al., 2015, 2017, 2020; Sangelantoni et al., 2022, among others), leading to a more realistic climate information.

This study describes a new series of 32-year high-resolution climate datasets for Sierra Nevada (SN), a Mediterranean mountain range in the southern Iberian Peninsula (IP) that constitutes a double hotspot region. These datasets, together called HighResClimNevada, provide primary climatic variables, bioclimatic variables, and extremes indices in a region with scarce climatic information with quality due to the difficulty of access. Furthermore, HighResClimNevada provides information at unprecedented spatial resolution in this region, which is useful for studies focusing on the impacts of climate change on botany, ecology, and other disciplines. HighResClimNevada, derived from climate modeling using a CPM, is available for the period from January 1991–December 2022.

This paper is structured as follows: Sect. 2 describes the model configuration for the development of HighResClimNevada, data used as a reference for the evaluation of HighResClimNevada, and variables provided by HighResClimNevada. Section 3 displays and discusses the results of the HighResClimNevada evaluation, Sect. 4 describes the data and code availability, and Sect. 5 summarizes and concludes the main findings of this work.

2 Methods

2.1 Study region

SN, located in the Baetic System (latitude 36.93–37.20° N and longitude 3.53–2.65° W), is the southernmost mountain range on the European continent. It houses some of the highest peaks in the IP, including Mulhacén (3479 m) and Veleta (3396 m) (Oliva et al., 2022). SN is a clear example of semi-arid high mountains being considered a double hotspot re-

gion where Mediterranean and Alpine climates cohabit about 40 km apart (Polo et al., 2019). Due to its singular conditions, it is home to many endemic plant and animal species, is considered one of the most important European hotspots for biodiversity (Blanca et al., 1998), and is a good candidate as a global change observatory. For these reasons, it was designated a biosphere reserve by UNESCO in 1986, natural park in 1989, and national park in 1999.

2.2 Climate model

HighResClimNevada has been developed using the Weather Research and Forecasting (WRF) model version 4.3.3 (Skamarock et al., 2021). This model was chosen for its ability to accurately characterize climate variables such as precipitation in complex topographical regions such as the IP, particularly for spatial resolutions of a few kilometers (i.e., grid spacing < 4 km, convection-permitting mode). To do that, a one-way double-nested configuration with a 5 : 1 nesting ratio (Fig. 1) was chosen: a parent domain (d01), which spans the whole IP with 5 km spatial resolution, and a nested domain (d02) covering SN with 1 km spatial resolution. In order to preserve a resolution step lower than 12 (Denis et al., 2003), we adopt a multi-nest approach. This avoids the necessity of a large spin-up zone in our simulation. We have followed, therefore, the recommendation of authors such as Matte et al. (2016), who pointed out double-nested configurations in a trade-off between quality and computational cost. On the other hand, the use of a one-way strategy was based on previous studies such as Messmer et al. (2021), who, in addition, found that a two-way strategy affects the representation of the domain when convection is disabled. The Lambert projection was used with the center at 37.65° N, 3.97° W and with 320×320 and 576×326 grid points in the west–east and south–north directions for d01 and d02, respectively. In the vertical, both domains were configured using 46 hybrid levels, with the top set to 50 hPa.

WRF was updated every 6 h using the fifth-generation European ReAnalysis (ERA5, Hersbach et al., 2020), the latest reanalysis product from the European Centre for Medium-Range Weather Forecasts, which has been shown to be effective for regional climate downscaling. Although ERA5 provides hourly data, we opted for a 6 h update frequency to allow the model a certain degree of free evolution (González-Rojí et al., 2022). Additionally, using hourly data for a 32-year climate simulation would be impractical due to the high storage and computational demands. To complete the entire period (1991–2022), the simulation was divided into 11-year runs, with the first year of each simulation being the spin-up of the model. This spin-up period was selected to balance the impact on simulations when a short spin-up period is used and the computational cost of CPM simulations. In this regard, a study conducted by Jerez et al. (2020) found that for atmospheric variables such as precipitation and temperature, a relatively short spin-up time (~ 1 week) is required.

However, soil variables need longer periods to reach such an equilibrium, and they depend on the initial soil moisture conditions and soil depth, among others (Khodayar et al., 2015). In this context and considering the trade-off between suitability and computational resources, as well as the fact that this study uses ERA5 data as lateral boundary conditions (LBCs), 1 year as spin-up was finally used.

For the selection of physical schemes, we applied the configuration suggested by Solano-Farías et al. (2024). This configuration was achieved by performing a sensitivity study resulting from combining different microphysics and convection schemes in the parent domain (d01); i.e., convection was switched off in the inner domain (d02) for all experiments. As a result, 12 WRF simulations of 1 year in length were completed and compared with different reference datasets in terms of precipitation and maximum and minimum temperatures. From that work, the authors concluded that the combination of parameterizations composed by the WRF single-model 7-class (WSM7, Bae et al., 2019), Grell–Freitas (Grell and Freitas, 2014) for convection in the parent domain (d01), the Community Atmosphere Model 3.0 (CAM3.0, Collins et al., 2004) for both long- and short-wave radiation, the Asymmetric Convective Model version 2 (ACM2, Pleim, 2007) for the planetary boundary layer (PBL), and the multiparametric Noah (NOAH-MP, Yang et al., 2011) land surface model (LSM) leads to an adequate characterization of climate conditions over Andalusia. A summary of the model configuration can be seen in Table 1.

2.3 Reference datasets

Observational datasets, although valuable, are not error-free, particularly in mountainous regions, where uncertainties tend to be more pronounced (Prein and Gobiet, 2017). Thus, daily values of precipitation (pr) and maximum, mean, and minimum temperature (tasmax, tasmean, and tasmin, respectively) from different sources were used (Table 2) to evaluate the HighResClimNevada performance, avoiding drawing incorrect conclusions due to observational uncertainties.

Satellite-based precipitation estimations were considered a source of precipitation information. The United States Global Precipitation Measurement (GPM) team and the National Aeronautics and Space Administration (NASA) of United States developed the Integrated Multi-SatellitE Retrievals (IMERG) for GPM version 6 (Huffman et al., 2019, 2020). This half-hourly multi-satellite-based product provides precipitation estimates for almost the entire planet with a spatial resolution of 0.1° and for a period from 2000–2021. Among the different versions, the IMERG Final Run was selected, which is calibrated at a monthly scale using the $1° \times 1°$ Global Precipitation Climatology Centre (GPCC) monthly monitoring product. On the other hand, the Satellite Precipitation Climate Prediction Center morphing method (CMORPH, Joyce et al., 2004) is a high-quality, high-resolution (~ 8 km of spatial resolution and a half-

https://doi.org/10.5194/essd-17-2809-2025

Earth Syst. Sci. Data, 17, 2809–2829, 2025
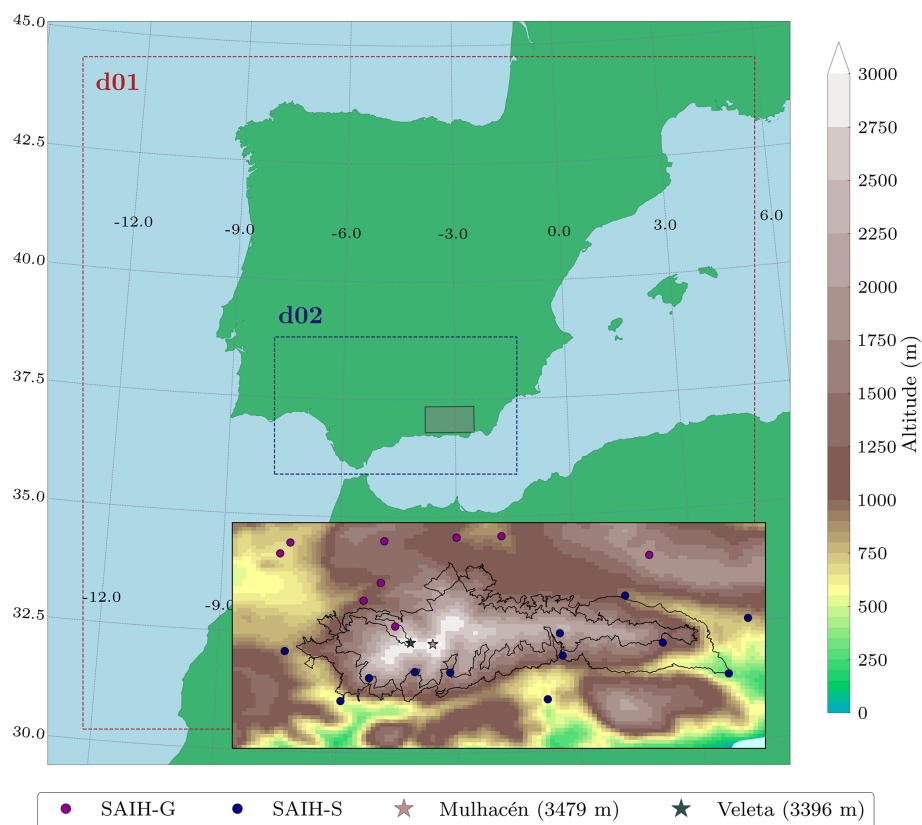
Figure 1. WRF domain configuration with two one-way domains: the parent domain (d01), which covers the Iberian Peninsula (IP) with 5 km spatial resolution, and the inner domain (d02), which spans the Andalusia region with 1 km spatial resolution. The area covered by HighResClimNevada is depicted in the insert in the bottom right, including the boundaries of both the natural and national parks of Sierra Nevada (black contours). The shading colors in this subfigure denote the elevation stated in meters above mean sea level, while the dots represent the locations of stations from the HidroSur automatic Hydrological Information System (SAIH-S) and the Guadalquivir automatic Hydrological Information System (SAIH-G).

hourly time frequency) dataset developed by the National Oceanic and Atmospheric Administration (NOAA) of the United States. CMORPH, which is derived from low-orbiter satellite microwave measurements, is available for the period from 1998 to the near present for the latitudinal bands from 60° N–60° S. The Climate Hazards group InfraRed Precipitation with Stations data (CHIRPS, Funk et al., 2015) includes gridded products that provide precipitation estimates for latitudinal bands between 50° S and 50° N. These data combines satellite precipitation data from NASA and NOAA with in situ station data from public and commercial archives. The global daily CHIRPS v2 with 0.05° spatial resolution, available since 1981, was used.

Additionally, gridded station-based products were used. On the one hand, meteorological gridded products developed by Peral et al. (2017) version 2 (referred to as RO-CIO_IBEB) were used. These daily datasets are the result of interpolating high-quality observational time series from the Spanish Meteorological Agency's (AEMET) National Bank of Climatological Data. ROCIO_IBEB provides precipitation and extreme temperature (maximum and mini-

mum) values for peninsular Spain and Balearic Islands at a 5 km spatial resolution from 1951–2022. On the other hand, a monthly precipitation dataset (UGR-SNGrid) developed by the Atmospheric Physics Group at the University of Granada (Romero-Jiménez et al., 2024) was also employed. UGR-SNGrid is a gridded dataset covering the SN Natural Park and its surroundings from 1990–2020, with a spatial resolution of 200 m. For its development, precipitation records from the ClimaNevada database (https://climanevada.obsnev.es/, last access: 13 January 2024) and the automated Hydrological Information System (SAIH) network were subjected to rigorous quality control before being spatially interpolated using the R package RegRAIN version 0.1.0 (Alzate Velásquez et al., 2017). Based on the Regionalisierte Niederschlage (REGNIE) method (Rauthe et al., 2013), RegRAIN combines multiple linear regression considering orographical factors such as location, slope, elevation, and inverse distance weighting. The orographical factors were obtained from a digital elevation model, and monthly regressions are calculated using precipitation time series from stations. More

Table 1. Main characteristics of the WRF model configuration applied to create the HighResClimNevada data.

	Parent domain (d01)	Nested domain (d02)
Regional climate model		
WRF-ARW v4.3.3 (Skamarock et al., 2021)		
Lateral boundary conditions		
ERA5 Reanalysis (Hersbach et al., 2023) every 6 h		
Domain configuration		
Nesting strategy	One-way	
Spatial resolution	5 km	1 km
Coverage	Iberian Peninsula	Andalusia
Dimensions (grid points)	320×320	576×326
Vertical coordinate system	Hybrid	Hybrid
Number of vertical levels	46	46
Model top pressure	50 hPa	50 hPa
Time step	30 s	6 s
Parameterization schemes		
Land surface model	Noah MP (Yang et al., 2011)	Noah MP (Yang et al., 2011)
Planetary boundary layer	ACM2 (Pleim et al., 2007)	ACM2 (Pleim et al., 2007)
Convection	GF (Grell and Freitas, 2014)	OFF
Microphysics	WSM7 (Bae et al., 2019)	WSM7 (Bae et al., 2019)
Long-wave radiation	CAM3 (Collins et al., 2004)	CAM3 (Collins et al., 2004)
Short-wave radiation	CAM3 (Collins et al., 2004)	CAM3 (Collins et al., 2004)
Atmospheric surface layer	Revised MM5 (Jiménez et al., 2012)	Revised MM5 (Jiménez et al., 2012)
Spin-up time	1 year	1 year

details about this methodology can be found in Romero-Jiménez et al. (2023).

Reanalysis data were employed as an additional source of information that would complement the sparse station network in this area. On the one hand, the global ERA5-Land reanalysis (Muñoz-Sabater et al., 2021) provides climatic and land-related variables with a 9 km spatial and hourly time step. It was developed using ERA5 as atmospheric forcing and is available from January 1950 to the near present. Additionally, the Copernicus European Regional ReAnalysis products (CERRA and CERRA-Land) were used. Both regional products are high-resolution reanalysis developed using dynamical downscaling methods. The CERRA reanalysis (Schimanke et al., 2021) employs HARMONIE-ALADIN as a limited-area numerical weather model, which is driven by ERA5, and the CERRA system to assimilate a dense network of in situ observations and satellite information. CERRA-Land (Verrelle et al., 2022), on the other hand, employs the land surface model SURFEX v8.1, which is run offline and forced using 3 h CERRA atmospheric variables and the daily surface precipitation from the MESCAN system. CERRA and CERRA-Land have the same integration domain (e.g., orography and coverage) and provide surface variables with 5.5 km spatial resolution from 1984–2021.

Precipitation and temperature data from weather stations have also been used for the evaluation of HighResClimNevada. Hourly data from the Automatic Hydrological Information System (SAIH) HidroSur (SAIH-S, http://www.redhidrosurmedioambiente.es, last access: 12 September 2024) and Guadalquivir (SAIH-G, https://www.chguadalquivir.es, last access: 16 September 2024), which are networks of high-quality stations with hourly precipitation and temperature data from 1997 and 2001, respectively, to the present, were used. To preserve as much quality climate data as possible, SAIH-G and SAIH-S time series with at least 85 % of records for a period of at least 19 years within the study period were used. For precipitation, the SAIH-S and SAIH-G stations selected were stations 9 and 13, respectively. For temperature, however, two stations were selected and only from SAIH-S.

All these databases were downloaded at their native temporal resolution for the time period covered by HighResClimNevada and then aggregated to the daily scale in cases where the resolution differed.

Table 2. Precipitation and temperature datasets used as reference in the evaluation of HighResClimNevada, classified according to their origin. Each reference database is identified by its name. Additionally, their spatial coverage, resolution (gridded products) or number of stations (punctual stations), temporal aggregation, available period (used), and studied variables are also shown. Pr, tasmax, tasmean, and tasmin denote daily accumulated precipitation and maximum, mean, and minimum temperatures, respectively. Hourly mean temperature is denoted as ta in order to differentiate it from daily values.

Name	Coverage (resolution or number or stations for pr (ta))	Temporal frequency	Available (analysis) period	Variable
Gridded dataset developed with in situ stations				
ROCIO_IBEB	Peninsular Spain and Balearic Islands (0.05°)	daily	1951–2022 (1991–2022)	pr, tasmax, tasmin
UGR-SNGrid	Sierra Nevada (200 m)	monthly	1990–2020 (1991–2020)	pr
Satellite-derived gridded products				
CMORPH	Latitudinal bands from 60° N and 60° S (8 km)	half-hourly	1998–present (1998–2022)	pr
GPM IMERG	Quasi global (0.1°)	half-hourly	2000–2021 (2001–2020)	pr
CHIRPS	Latitudinal bands from 50° N to 50° S (0.05°)	daily	1981–present (1991–2022)	pr
Reanalysis gridded products				
ERA5-Land	Global (∼ 9 km)	1 h	1950–present (1991–2022)	pr, ta
CERRA	Europe (5.5 km)	3 h	1984–2021 (1991–2021)	ta
CERRA-Land	Europe (5.5 km)	daily	1984–2021 (1991–2021)	pr
Punctual in situ stations				
Automatic Hydrological Information System (SAIH) stations	Guadalquivir (SAIH-G, 9) and southern (SAIH-S, 13 (2)) hydrological basins	1 h	SAIH-G: 2001–present (2001–2022), SAIH-S: 1997–present (1997–2022)	pr, ta

2.4 Climate variables in HighResClimNevada: format and file organization

HighResClimNevada has been structured in netCDF files that contain 3D climate fields (time × latitude × longitude) covering longitude from 3.85–2.40° W and latitude from 36.50–37.50° N (see Fig. 1). These data are provided in the original Lambert grids for a period from January 1991 to December 2022. All files also provide a 2D mesh with the altitude (z) at sea level expressed in meters above the mean sea level and includes variables over land. The database is divided into (1) primary climate variables, (2) bioclimatic variables, (3) extreme ETCCDI climate indices, and (4) precipitation-hour extreme variables.

2.4.1 Primary climate variables

- *Near-surface temperature (ta, °C).* Temperature plays a crucial role in ecosystem functions being variables commonly used to describe the climate in a region. Near-surface (2 m) temperature was obtained from raw simulation outputs with a 10 min temporal resolution. Then, hourly (ta) and daily mean of the maximum (tasmax), mean (tasmean), and minimum (tasmin) temperatures were calculated based on these values.

- *Precipitation (pr, $kg\,m^{-2}$).* The accumulated precipitation amounts were obtained from raw 10 min WRF outputs. As for temperature, these values were then aggregated on hourly and daily scales to be part of the HighResClimNevada datasets.

- *Near-surface relative humidity (hur, %).* Changes in humidity over land also have important implications on ecosystems. Near-surface temperature (ta, °C), 3 h outputs of water vapor mixing ratio at 2 m (r, $kg\,kg^{-1}$), and surface pressure (ps, hPa) provided by WRF were used to estimate hur using Eqs. (1)–(3).

$$e_s = 6.11 \times 10^{\frac{7.5(ta-273.15)}{(ta-273.15)+237.3}}, \tag{1}$$

$$r_s = \frac{0.622 e_s}{ps - e_s}, \tag{2}$$

$$hur = \frac{r}{r_s} \times 100, \tag{3}$$

where e_s is the water vapor pressure and r_s is the saturated mixing ratio in $kg\,kg^{-1}$. Then, 3 h hur was used to estimate the daily averages.

- *Surface pressure (ps, Pa).* Atmospheric pressure was averaged at a daily scale using the corresponding 3 h surface pressure from WRF outputs.

– *Surface net radiation (net_radiation, $W\,m^{-2}$)*. It is the radiant energy available at the surface to perform work inside the ecosystem, and it is critical for maintaining biological and physical processes. Surface net radiation is calculated as the balance between the absorbed, reflected, and emitted energy by the Earth's surface using 3 h outputs and following Eq. (4).

$$\text{net\_radiation} = (R_s \downarrow - R_s \uparrow) + (R_l \downarrow - R_l \uparrow), \qquad (4)$$

where $R_{s\downarrow}$ ($W\,m^{-2}$) is the incoming solar radiation, $R_{s\uparrow}$ ($W\,m^{-2}$) is the proportion of the solar radiation reflected by the surface, $R_{l\downarrow}$ ($W\,m^{-2}$) is the incoming long-wave radiation emitted by the atmosphere, and $R_{l\uparrow}$ ($W\,m^{-2}$) is the radiation emitted by the surface.

– *Surface wind speed (wind_speed, $m\,s^{-1}$)*. The daily 10 m wind speed was calculated using 3 h outputs of U10 ($m\,s^{-1}$) and V10 ($m\,s^{-1}$), which are the eastward and northward WRF wind components at 10 m, respectively, using Eq. (5).

$$\text{wind\_speed} = \sqrt{U10^2 + V10^2} \qquad (5)$$

2.4.2 Bioclimatic variables

Based on monthly temperature values and precipitation, bioclimatic variables have been calculated and are available at an annual scale in the HighResClimNevada database. These indices, which describe the ecological and environmental status of ecosystems, were obtained following BIOCLIM WorldClim (Fick and Hijmans, 2017; Hijmans et al., 2005), CHELSA Bioclim (Karger et al., 2017), and CMCC-BioClimInd (Noce et al., 2020) standard definitions. Here, we considered those bioclimatic variables with interest for semi-arid mountains and due to their relevance in agricultural and ecological applications, which are

– *Annual mean temperature (BIO1, °C)*. It is calculated for each year by averaging tasmean. Similarly, seasonal values have been considered, with summer (June, July, August, JJA) and winter (December, January, February, DJF) representing the dry/warm and wet/cold seasons, respectively. This variable was also considered for spring (March, April, May, MAM) and autumn (September, October, November, SON) to reflect intermediate seasons. Additionally, the annual average of tasmax ($BIO1_{max}$) and tasmin ($BIO1_{min}$) were calculated as well as the subsequent values for each season.

– *Mean diurnal range (DTR or BIO2, °C)*. It is the difference between the monthly tasmax and tasmin. In this work, BIO2 is referred to as DTR as defined by the ETCCDI as an extreme index of temperature. That is, the daily difference between tasmax and tasmin was calculated to obtain annual means of DTR.

– *Isothermality (BIO3, %)*. It measures the degree of daily temperature fluctuations (BIO2) compared to annual variations throughout extreme months (BIO7) according to Eq. (6).

$$\text{BIO3} = \frac{\text{BIO2}}{\text{BIO7}} \times 100 \qquad (6)$$

– *Temperature seasonality (BIO4, °C)*. It refers to temperature fluctuations throughout the year. BIO4 is computed as the standard deviation of monthly tasmean, which is obtained using the 12-monthly values from each year (Noce et al., 2020).

– *Maximum temperature of the warmest month (BIO5, °C)*. It is defined through the monthly means of tasmax. Thus, for each year, the monthly tasmax value of the month with the highest temperature is selected as the maximum temperature of the warmest month of that year.

– *Minimum temperature of the coldest month (BIO6, °C)*. Similarly to BIO5, monthly means of tasmin are computed throughout the years, and then minimum values for each year are taken as the minimum temperature of the coldest month.

– *Annual temperature range (BIO7, °C)*. It reflects the range of temperatures between the coldest and the warmest months.

$$\text{BIO7} = \text{BIO5} - \text{BIO6} \qquad (7)$$

– *Mean temperature of the wettest quarter (BIO8, °C)*. The wettest quarters were obtained using as a reference the spatial mean of HighResClimNevada pr in the SN Natural Park. For each year, the 3-month precipitation moving sum is calculated, and the maximum value is determined through its central month. BIO8 is then calculated as the average tasmean of the three consecutive averages starting in the wettest quarters (Noce et al., 2020).

– *Mean temperature of the driest quarter (BIO9, °C)*. Similarly to BIO8, the driest quarter is obtained for each year looking for the minimum 3-month moving sum determined through its central month. Then, mean temperatures for each year are computed through the 3 consecutive months, starting in the driest quarters.

– *Annual precipitation (BIO12, $kg\,m^{-2}$)*. The total amount of precipitation was computed as the average of the annual sum of precipitation. Similarly to temperature, seasonal values ($BIO12_{XXX}$ with XXX being DJF, MAM, JJA, or SON) were obtained.

– *Precipitation of wettest month (BIO13, $kg\,m^{-2}$)*. Similarly to BIO5, it is computed as the highest monthly sum of precipitation for each year.

– *Precipitation seasonality (BIO15, %)*. It shows the precipitation variations throughout the year, and it is calculated as the coefficient of variation in monthly values in each year (Eq. 8), expressed as a percentage.

$$\mathrm{BIO15} = \frac{s_{\mathrm{pr}}}{\overline{\mathrm{pr}}} \times 100, \tag{8}$$

where s_{pr} is the annual standard deviation and $\overline{\mathrm{pr}}$ is the mean.

– *Precipitation of coldest quarter (BIO19, $kg\,m^{-2}$)*. This metric is considered since SN serves as a "water tower" for neighboring regions. Similarly to BIO8 and BIO9, coldest quarters of each year are determined as the lowest temperature of the 3-month moving average from HighResClimNevada. For each year, the precipitation amount is then calculated for the 3 consecutive months starting in the coldest quarters.

2.4.3 Extreme ETCCDI climate indices

Temperature and precipitation extremes indices from the Expert Team on Climate Change, Detection, and Indices (ETC-CDI, Frich et al., 2002) were also calculated. Here, extreme variables with relevance in mountain ecosystems have been considered, and these are as follows:

– *Warmest day (TXx, °C) and coldest night (TNn, °C)*. TXx represents the maximum value of tasmax in the warmest month. In the same way, TNn is understood as the lowest value of tasmin in the coldest month.

– *Growing season length (GSL, days)*. The growth season is the time of year when plants grow effectively. According to the ETCCDI, GSL is defined as the number of days per year between the first occurrence of at least 6 d with tasmean $> 5\,°C$ and the first occurrence (after 1 July) of 6 d with tasmean $< 5\,°C$.

– *Icing days (ID, days) and frost days (TNltm2, days)*. Here, mountainous cold extreme patterns are represented by the icing days (annual number of days with tasmax $< 0\,°C$) and frost days (annual number of days with tasmin $< -2\,°C$). Note that the original definition for frost day has a threshold of tasmin $< 0\,°C$, but in the SN high-mountain region, a more extreme threshold must be considered.

– *Wet, heavy, and very heavy precipitation days (R1mm, R10mm, and R20mm, expressed in $d\,yr^{-1}$)*. The frequency of extreme precipitation is explored through the number of days per year with pr $> 1\,mm$ (wet days), pr $> 10\,mm$ (heavy precipitation days), and pr $> 20\,mm$ (very heavy precipitation days).

– *Simple daily intensity index (SDII, $kg\,m^{-2}$) and wettest pentad (rx5d, expressed in $kg\,m^{-2}$)*. SDII calculates the mean daily pr on wet days (pr $> 1\,mm$) for a year and rx5d is the highest total quantity of pr falling on 5 consecutive days. These indices are calculated as a proxy for the magnitude of daily extreme precipitation.

– *Consecutive dry days (CDD, expressed in $d\,yr^{-1}$)*. This is the longest period in a year of consecutive days with less than 1 mm of pr per day. The significance of this index lies in the fact that it serves as a drought indicator, which is a very relevant aspect in a semi-arid region such as SN.

2.4.4 Precipitation-hour extreme indices

Finally, very extreme precipitation events were also considered through precipitation-hour indices, which are the following:

– *Wet-hour frequency ($F_{\mathrm{wet\text{-}hour}}$, %)*. It is the percentage of hours per year corresponding to wet hours (pr $> 0.1\,mm$).

– *Wet-hour intensity ($I_{\mathrm{wet\text{-}hour}}$, $kg\,m^{-2}$)*. This refers to the average amount of precipitation in 1 h only considering wet hours (pr $> 0.1\,mm$).

– *Maximum amount of precipitation in the wettest month (PRWw, $kg\,m^{-2}$)*. Following the philosophy of ETCCDI extremes such as TXx or TNn, PRWw is calculated by determining the maximum amount of precipitation in each month, and then the maximum value is determined for each year to obtain the PRWw time series.

3 Results

3.1 Temperature and precipitation distributions

Figure 2 shows the probability density functions (PDFs) of tasmean (Fig. 2a) and pseudo-PDFs of pr (Fig. 2b) as well as the annual cycles of monthly values of both variables (Fig. 2c and d) for reference climate datasets and HighResClimNevada. WRF data from the parent domain (05-WRF) have also been included because they are closer in spatial resolution to the reference datasets and hence more comparable. To obtain the PDFs, pseudo-PDFs, and annual cycles, all grid points in the SN Natural Park were considered. PDFs were estimated using a 0.5 °C bin, whereas pseudo-PDFs were obtained using an approach similar to that provided in Argüeso et al. (2012). That is, considering all grid points within the national and natural park borders, pseudo-PDFs for each dataset were obtained by grouping events of daily precipitation (pr $> 0.1\,mm$) into 2 mm bins. The number of events multiplied by the mean intensity for each bin was then determined by dividing the total precipitation amounts (expressed in mm) for each bin by the number of grid points and days. Pseudo-PDFs were selected instead

Table 3. Bioclimatic variables, ETCCDI, and precipitation-hour extreme indices available in HighResClimNevada. The table includes the name of the index, the variables involved, and time aggregation used for this calculation, the acronym for the index, and the units in which this is expressed.

| Name	Variable (time aggregation)	Acronym	Units
WorldClim bioclimatic variables			
Annual mean temperature	tasmean (monthly)	BIO1	°C
Annual means of maximum temperature*	tasmax (monthly)	BIO1max	°C
Annual means of minimum temperature*	tasmin (monthly)	BIO1min	°C
Seasonal mean temperature*	tasmean (monthly)	BIO1	°C
Seasonal mean of maximum temperature*	tasmax (monthly)	BIO1max	°C
Seasonal mean of minimum temperature*	tasmin (monthly)	BIO1min	°C
Isothermality	tasmean (monthly)	BIO3	%
Temperature seasonality	pr (monthly)	BIO4	°C
Maximum temperature of warmest month	tasmax (monthly)	BIO5	°C
Minimum temperature of coldest month	tasmin (monthly)	BIO6	°C
Annual temperature range	tasmax, tasmin (monthly)	BIO7	°C
Mean temperature in wettest quarter	tasmean (monthly)	BIO8	°C
Mean temperature in driest quarter	tasmean (monthly)	BIO9	°C
Annual precipitation	pr (monthly)	BIO12	$\mathrm{kg\,m^{-2}}$
Seasonal precipitation*	pr (monthly)	BIO12*	$\mathrm{kg\,m^{-2}}$
Precipitation of wettest month	pr (monthly)	BIO13	$\mathrm{kg\,m^{-2}}$
Precipitation seasonality	pr (monthly)	BIO15	%
Precipitation in the coldest quarter	pr (monthly)	BIO19	$\mathrm{kg\,m^{-2}}$
ETCCDI extreme indices			
Daily temperature range	tasmax, tasmin (daily)	DTR (BIO2)	°C
Warmest day	tasmax (daily)	TXx	°C
Coldest night	tasmin (daily)	TNn	°C
Growing season length	tasmean (daily)	GSL	$\mathrm{d\,yr^{-1}}$
Icing days	tasmax (daily)	ID	$\mathrm{d\,yr^{-1}}$
Frost days*	tasmin (daily)	TNltm2	$\mathrm{d\,yr^{-1}}$
Wet days	pr (daily)	R1mm	$\mathrm{d\,yr^{-1}}$
Heavy precipitation days	pr (daily)	R10mm	$\mathrm{d\,yr^{-1}}$
Very heavy precipitation days	pr (daily)	R20mm	$\mathrm{d\,yr^{-1}}$
Simple daily intensity	pr (daily)	SDII	$\mathrm{kg\,m^{-2}}$
Wettest pentad	pr (daily)	Rx5d	$\mathrm{kg\,m^{-2}}$
Maximum length of dry spell	pr (daily)	CDD	$\mathrm{d\,yr^{-1}}$
Precipitation-hour extreme indices			
Wet-hour frequency	pr (hourly)	$F_{\mathrm{wet\text{-}hour}}$	%
Wet-hour intensity	pr (hourly)	$I_{\mathrm{wet\text{-}hour}}$	$\mathrm{kg\,m^{-2}}$
Maximum amount in the wettest month	pr (hourly)	PRWw	$\mathrm{kg\,m^{-2}}$

Asterisks (*) indicate self-defined variables, which are based on original bioclimatic variables or ETCCDI indices.

of the traditional PDFs in order to avoid masking light precipitation and, more importantly, heavy precipitation events.

In general, HighResClimNevada tasmean shows similar PDFs to other climate products (values ranging from −15 to 35 °C) with certain bimodal features with two peaks of frequency (the highest peak around 5 °C, while the lighter one is around 20 °C). ROCIO_IBEB shows the greatest difference in the shape of the distribution, which exhibits a more diffuse bimodal character with its second mode shifted to-

wards higher values. In terms of precipitation (Fig. 2b), differences between pseudo-PDFs are shown depending on the spatial resolution and the nature of the data. Events with pr of around $10\,\mathrm{mm\,d^{-1}}$ seem to contribute to the highest amount of precipitation in HighResClimNevada. CHIRPS shows a similar shape in its pseudo-PDF but slightly shifted towards higher precipitation events. For the other climatic products, however, the highest amount of pr occurs for lighter events ($5\,\mathrm{mm\,d^{-1}}$ or less), which is more pronounced in GPM
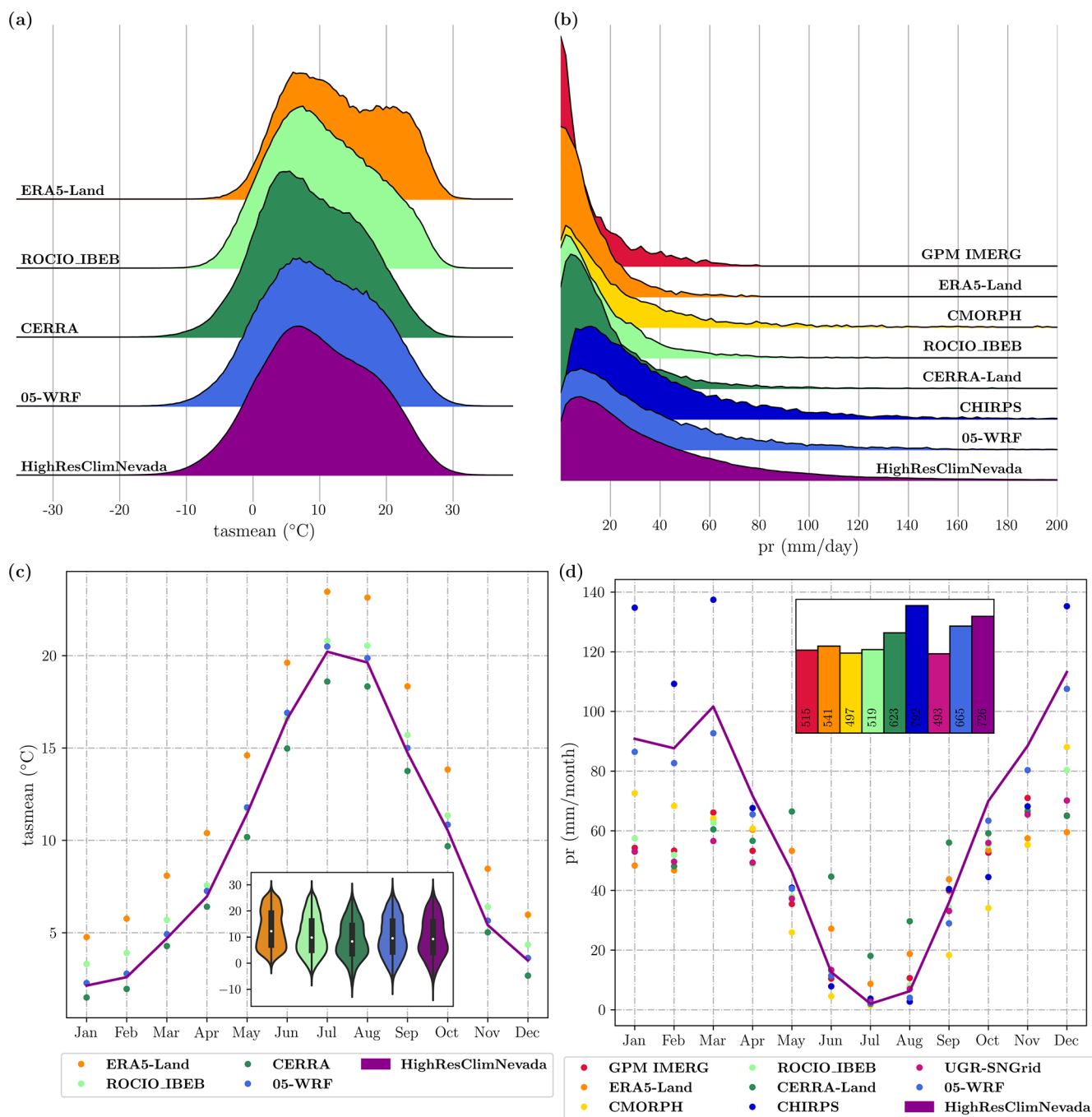
Figure 2. (a) Probability density functions (PDFs) of daily mean temperature (tasmean) and **(b)** pseudo-PDFs of the daily precipitation (pr) for all climatic products. Annual cycle of the monthly mean **(c)** temperature and **(d)** precipitation. The insert in **(c)** shows a violin plot with the monthly mean temperature values at each grid point and for each database. The insert in **(d)** shows a bar chart with the average annual precipitation amount (expressed in $mm\,yr^{-1}$) in each database.

IMERG and ERA5-Land. The latter suggests that the shape of the PDF is influenced, at least in part, by the spatial resolution of the data.

HighResClimNevada exhibits an annual cycle of monthly tasmean similar to 05-WRF and ROCIO_IBEB (Fig. 2c). However, underestimations of roughly 3 °C are shown com-

pared to ERA5-Land along with slight overestimations when CERRA is employed as a reference. In any case, all climatic products reveal an annual cycle with the highest temperature in July and the lowest in January. Concerning the spatiotemporal distribution of temperature, the violin plot in Fig. 2c shows that HighResClimNevada, 05-WRF, and

CERRA are more widespread, which could be related to the spatial resolution (the higher the spatial resolution, the greater the dispersion) and the nature of the data as these three climatic products are derived from modeled data. It should be noted that in high-mountain regions, the number of weather stations is limited, making temperature characterization more difficult for station-based products such as ROCIO_IBEB. Regarding precipitation, all climate products have a similar shape in their annual cycle (Fig. 2d), with the highest precipitation in December and the lowest during July. However, the amount of precipitation differs between months. HighResClimNevada produces a high amount of pr ($726\,\mathrm{mm\,yr^{-1}}$), second only to CHIRPS ($792\,\mathrm{mm\,yr^{-1}}$) (inner figure in Fig. 2d), which is due to a higher amount of pr throughout the autumn and winter months. However, compared to reanalysis-based data such as CERRA-Land or ERA5-Land, HighResClimNevada seems to reveal a smaller pr amount throughout the summer.

3.2 Temperature and precipitation bioclimatic variables and extremes

Figure 3 depicts the annual average of tasmax ($\mathrm{BIO1_{max}}$), tasmean (BIO1), and tasmin ($\mathrm{BIO1_{min}}$) for reference datasets (ERA5-Land, ROCIO_IBEB, and CERRA) and modeled data (05-WRF and HighResClimNevada). The dots in each panel represent the temperature recorded by SAIH stations. All climatic products are represented in their native spatial resolution to avoid problems caused by the interpolation method and the difference between spatial resolutions. Additionally, the temporal evolution of temperature in the natural park is depicted as warming stripes or standardized anomalies (i.e., annual temperature minus the annual mean in the common period, 2001–2020, divided by its standard deviation) under each map. Blue colors represent cooler-than-average years, while red colors suggest warmer-than-normal years. Blue and red intensities represent the magnitude of the anomaly. BIO1 characterizes the amount of energy captured by an ecosystem during a year, making its knowledge highly relevant for the conservation of high-mountain ecosystems. In general, results show that temperature values ($\mathrm{BIO1_{max}}$, BIO1, and $\mathrm{BIO1_{min}}$) are very influenced by elevation, with the lowest values over the highest mountain peaks. All climatic products exhibit both similar spatial patterns and interannual variability, with the latter being as shown by warming stripes. These results, moreover, evidence the effect of spatial resolution. That is, datasets with coarser spatial resolution show more homogeneous temperature patterns as they are not able to capture the elevation effects adequately. As a result, temperature in the Mulhacén and Veleta peaks in these datasets is usually higher (e.g., while ERA5-Land shows $\mathrm{BIO1_{min}}$ values around $7\,°\mathrm{C}$ in the highest altitudes, HighResClimNevada indicates values around $-2\,°\mathrm{C}$). Moreover, HighResClimNevada produces comparable values to those from SAIH stations, as observed in 05-WRF, CERRA, and

ROCIO_IBEB. However, ERA5-Land tends to overestimate both $\mathrm{BIO1_{max}}$, BIO1, and $\mathrm{BIO1_{min}}$. Comparable results can be found for seasonal values (Figs. S1–S4 in the Supplement).

HighResClimNevada, as other climatic products, accurately captures the main spatial patterns of annual precipitation in SN, showing an east–southwest gradient (Fig. 4). However, when we focus on high elevation areas, differences emerge that are determined by the spatial resolution and the nature of the data. Thus, in this region, downscaled fields (i.e., HighResClimNevada and 05-WRF), high-resolution satellite-derived products (CHIRPS), and high-resolution reanalysis (CERRA-Land) exhibit higher annual precipitation (greater than 1100 mm) than station-based data (ROCIO_IBEB and UGR-SNGrid), and others exhibit satellite-based and reanalysis data with a lower resolution (GPM IMERG and ERA5-Land), where annual precipitation ranges from 550–700 mm approximately. These findings suggest the importance of spatial resolution in representing this variable as datasets with resolutions of 5 km (or less) show a significant peak in annual cumulative precipitation at higher altitude. Lower-resolution datasets, on the other hand, exhibit more homogeneous precipitation patterns. This behavior is also shown in UGR-SNGrid and ROCIO_IBEB, where stations at high altitudes for precipitation calculation are very scarce. In comparison to the SAIH stations, HighResClimNevada shows higher BIO12, particularly at high altitude, where UGR-SNGrid produces closer values to these stations. It should be noted that the SAIH stations were one of the data sources in the development of UGR-SNGrid; therefore, similarities between the two are expected. It is also important to highlight the challenge of maintaining high-mountain weather stations due to their limited accessibility, especially during storm events, when observed values are likely to be lower than those actually occurring. As a result, we know that, while these stations are reasonably good, their geographical position limits their quality. Grids based on these values are so likely to inherit this type of problem. HighResClimNevada presents a general agreement with other climatic products in the interannual variability of precipitation, as shown by the drying stripes. Similar conclusions can be drawn regarding the amount of precipitation that falls on average during winter (Fig. S5 in the Supplement) and spring (Fig. S6 in the Supplement). For summer (Fig. S7 in the Supplement), all climatic products show precipitation values lower than 75 mm except for CERRA-Land and SAIH stations, which have precipitation values above 125 mm, although in different locations. For autumn (Fig. S8 in the Supplement), WRF outputs and CERRA-Land again show pr above 300 mm in the northwest, which is not replicated by other climatic products. However, for this season, the spatial pattern across the national park appears to be more accurate than in other climatic products when compared to SAIH stations.

https://doi.org/10.5194/essd-17-2809-2025

Earth Syst. Sci. Data, 17, 2809–2829, 2025
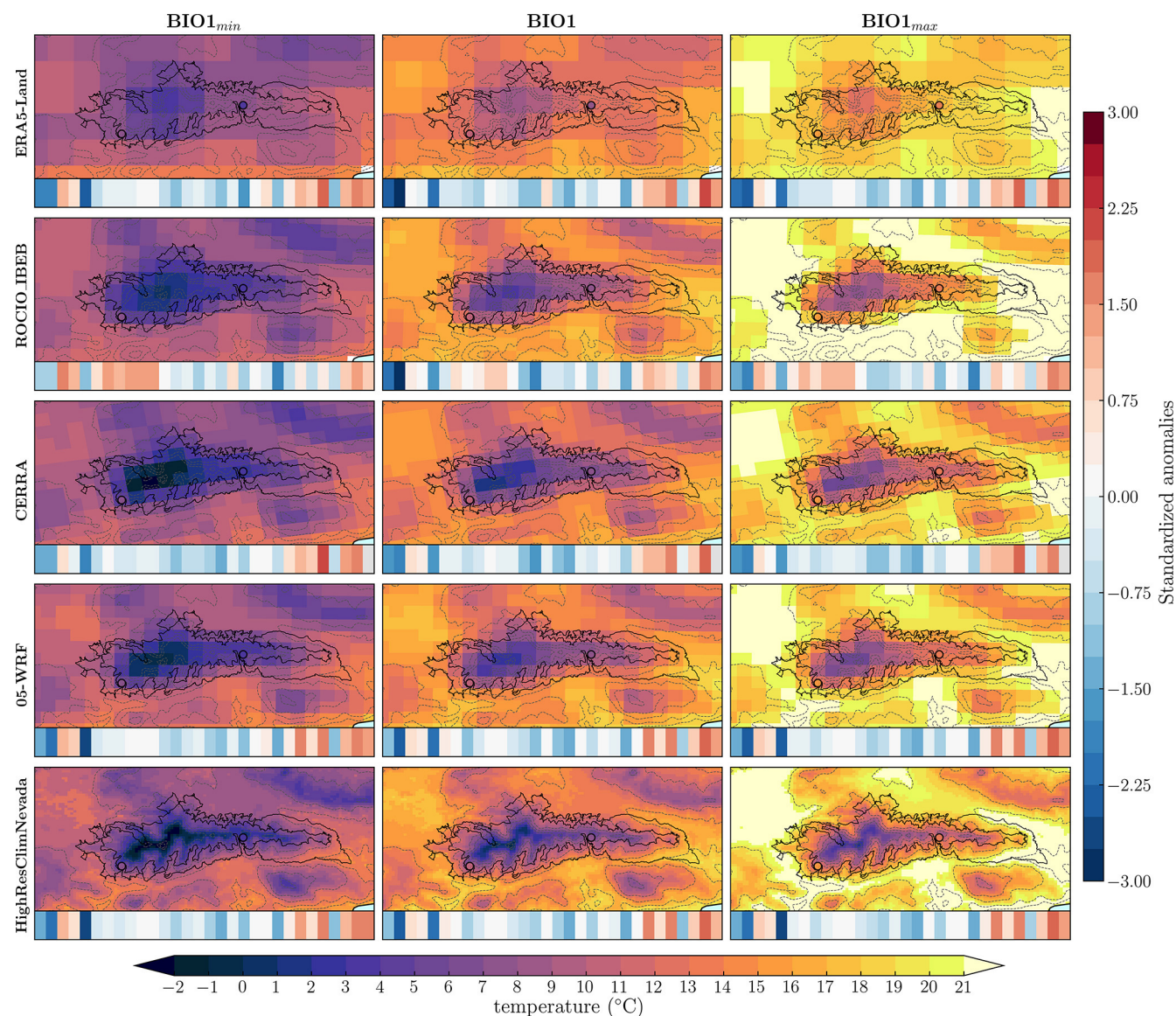
Figure 3. Annual average daily minimum, mean, and maximum temperatures (BIO1$_{min}$, BIO1, and BIO1$_{max}$) for each reference dataset (ERA5-Land, ROCIO_IBEB, and CERRA) and for downscaled data (05-WRF and HighResClimNevada). The dots in each panel represent the temperature recorded by SAIH stations, and the solid black lines display the national and natural park boundaries. Normalized anomalies for SN natural park over the period from 2001–2020 for each database are shown below the corresponding spatial map in the form of warming stripes. In this representation, red colors indicate positive standardized anomalies, and blue colors correspond to negative values compared to the mean value for the whole period.

Figure 5 depicts the long-term mean spatial patterns of temperature bioclimatic variables (Fig. 5a–5f) and ETCCDI extreme indices (Fig. 5g–5l) for HighResClimNevada. In each panel, dots represent the corresponding values for SAIH stations. In general, HighResClimNevada shows a comparable climate behavior to other products (Figs. S9–S12 in the Supplement) and stations but with an apparent improvement due to the enhanced resolution. That is, HighResClimNevada characterizes orography-related effects that are not well captured by coarser climatic products like ERA5-Land (Fig. S9).

In this regard, elevation influences most of the bioclimatic variables and extremes except for BIO4 and BIO7. Isothermality (BIO3, Fig. 5a) is a bioclimatic measure that compares variability within the day (BIO2 or DTR, Fig. 5g) to variability throughout the year (BIO7, Fig. 5c). BIO3 is crucial for ecosystems as many species might suffer damage in their population distribution as a result of daily and annual oscillations (O'Donnell and Ignizio, 2012). Values above 100 % indicate that daily temperature variability is equal to the annual variability. According to HighResClimNevada,
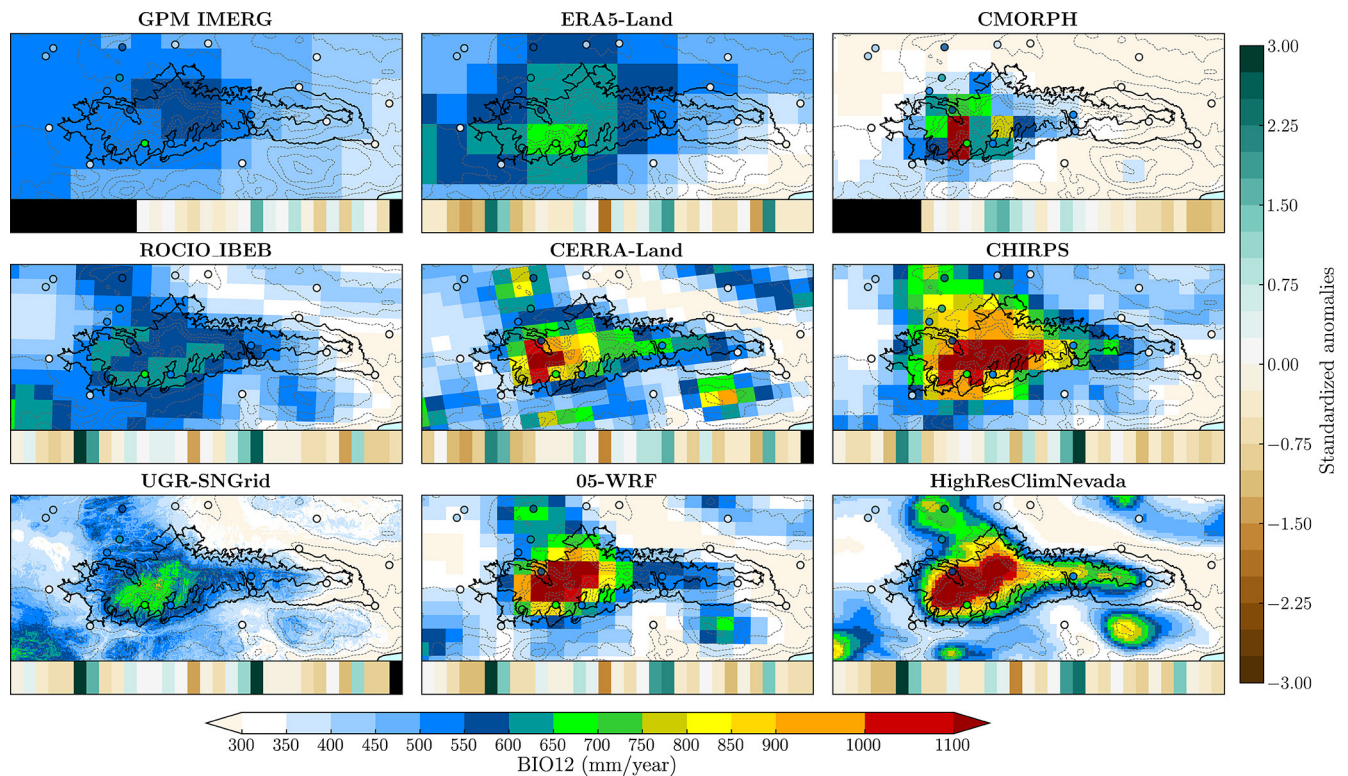
Figure 4. Average annual precipitation (BIO12, $mm\,yr^{-1}$) for station-based data (ROCIO_IBEB and UGR-SNGrid), satellite image-based data (GPM IMERG, CMORPH, and CHIRPS), reanalysis data (ERA5-Land and CERRA-Land), and downscaled precipitation data (05-WRF and HighResClimNevada). The dots in each panel represent the precipitation recorded by SAIH stations, and the solid black lines display the national and natural park boundaries. The annual standardized anomalies over the period from 2001–2020 for each database are shown below the corresponding spatial map in the form of drying stripes. In this representation, green colors indicate wet anomalies and brown colors the negative ones. Black colors indicate no data for that year.

SN has low BIO3 (up to 35 %), indicating that temperature fluctuations in this region during the day account for no more than 35 % of the total variation across the year. The lowest BIO3 values are depicted over the highest peaks, where they reach values less than 25 %. In this region, DTR is also the lowest in this region, with values falling below 6 °C. BIO7, however, reaches values between 23 °C and 30 °C, with the maximum located in the northeast of the SN Natural Park. Like BIO7, temperature seasonality (BIO4) illustrates the temperature variability throughout the year. HighResClimNevada (Fig. 5b), with values between 6 and 7 °C, has the highest BIO4 values in the northeastern part of the natural park. For this variable, although the results of other climatic products are within the same range, their spatial patterns differ significantly. BIO5 (Fig. 5d), BIO8 (Fig. 5e), and BIO9 (Fig. 5f) are useful when we are interested in analyzing if species distributions are affected by warm, wet, and dry temperatures, respectively (O'Donnell and Ignizio, 2012). Although HighResClimNevada is comparable to other climatic products in terms of these variables (see Figs. S9–S12d, S9–S12e, and S9–S12f), it appears to show lower values, especially when compared to ERA5-Land and RO-

CIO_IBEB, to be higher at the highest peaks. Similarly, HighResClimNevada has higher TNltm2 (Fig. 5l) and ID (Fig. 5k) than other climatic products, with values exceeding 160 and 105 $d\,yr^{-1}$, respectively. TNltm2 and ID have critical significance for ecosystems as prolonged cold temperatures may cause considerable damage, affecting the survival of plant and animal species (Liu et al., 2018). GSL is a key variable in vegetable ecosystems because it influences essential functions including hydrology, nutrient cycling, productivity, and climate feedback (Barnard et al., 2018). In terms of this variable, HighResClimNevada shows values varying from 270 $d\,yr^{-1}$ in the outermost parts of the SN Natural Park to values below 90 $d\,yr^{-1}$ at the highest peaks (Fig. 5j), which is very similar to other climate products.

Figure 6 depicts the interannual climate variability of bioclimatic variables and temperature extreme ETCCDI indices through the normalized anomalies in the area delimited by the SN Natural Park and estimated using the mean and standard deviation during the common period (2001–2020). For each index, the four databases, i.e., the three reference temperature datasets and HighResClimNevada, are plotted according to the order defined by the legend, with the color
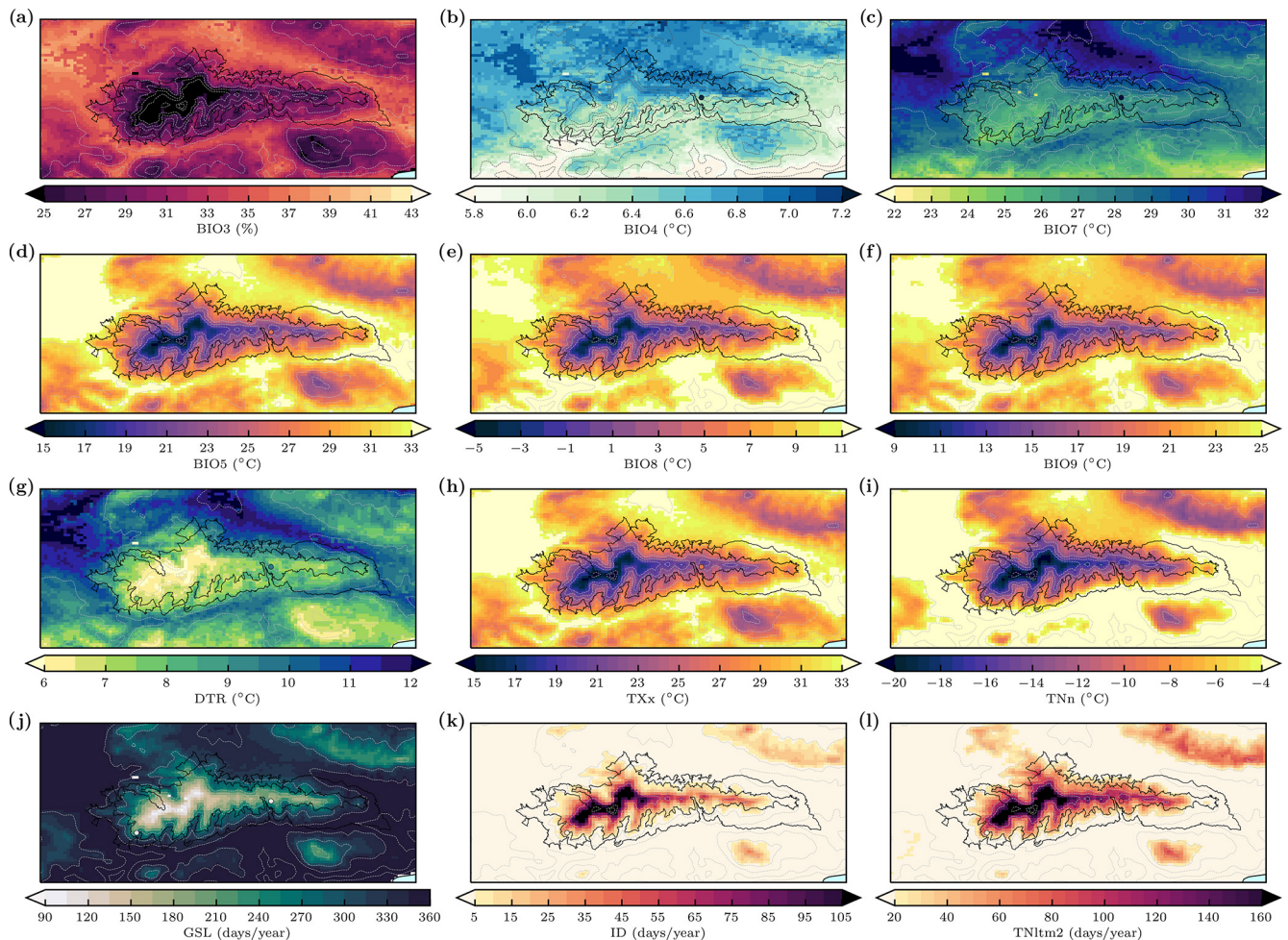
Figure 5. Spatial patterns of temperature bioclimatic variables and extreme ETCCDI indices in HighResClimNevada. **(a)** Isothermality (BIO3,%), **(b)** temperature seasonality (BIO4, °C), **(c)** annual temperature range (BIO7, °C), **(d)** maximum temperature of the warmest month (BIO5, °C), **(e)** mean temperature of the wettest quarter (BIO8, °C), **(f)** mean temperature of driest quarter (BIO9, °C), **(g)** daily temperature range (DTR, ° C), **(h)** maximum warmest day (TXx, °C), **(i)** minimum coldest night (TNn, °C), **(j)** growing season length (GSL, d yr^{-1}), **(k)** icing days (ID, d yr^{-1}), and **(l)** frost days (TNltm2, d yr^{-1}). The dots in each panel reflect the values achieved by SAIH stations, while the black solid lines display the national and natural park boundaries.

in each triangle representing the normalized anomaly for that year. Triangles colored in shades of red indicate that the index takes a value above normal, and blue follows the opposite pattern. In this figure, grey triangles indicate that there are no values in that dataset for that year. Overall, HighResClimNevada has a very similar temporal evolution to other climate products in terms of bioclimatic variables (from BIO3 to BIO9), suggesting that it is able to capture the SN temperature interannual variability. Thus, in general, anomalies in HighResClimNevada coincide in not only sign with those from other climatic products, but also magnitude. That is, all climatic products exhibited very high (low) BIO3 anomalies in 1997 (2012), with BIO7 being lower (higher) than normal. Note that BIO7 is the denominator for BIO3. This result indicates a small (high) dispersion in monthly temperature in that year when compared to the long-term cli-

mate, which is corroborated by BIO4. In the same way, BIO5 and BIO6 also agree in all products for 1997 (2012), showing that the maximum temperature of the warmest month was lower (higher) than normal and that the minimum temperature of the coldest month was higher (lower) than normal. Moreover, these years showed an unusually low (high) temperature in the driest quarter for that year, as indicated by BIO9. In the same way, temperature extremes are also similar in all climatic products, also suggesting that HighResClimNevada captures the interannual variability of extreme temperature.

Precipitation bioclimatic variables and extremes for HighResClimNevada are represented in Fig. 7. The dots in each panel reflect the values achieved by SAIH stations, while the solid black lines display the national and natural park boundaries. In general, the results suggest that orography influ-
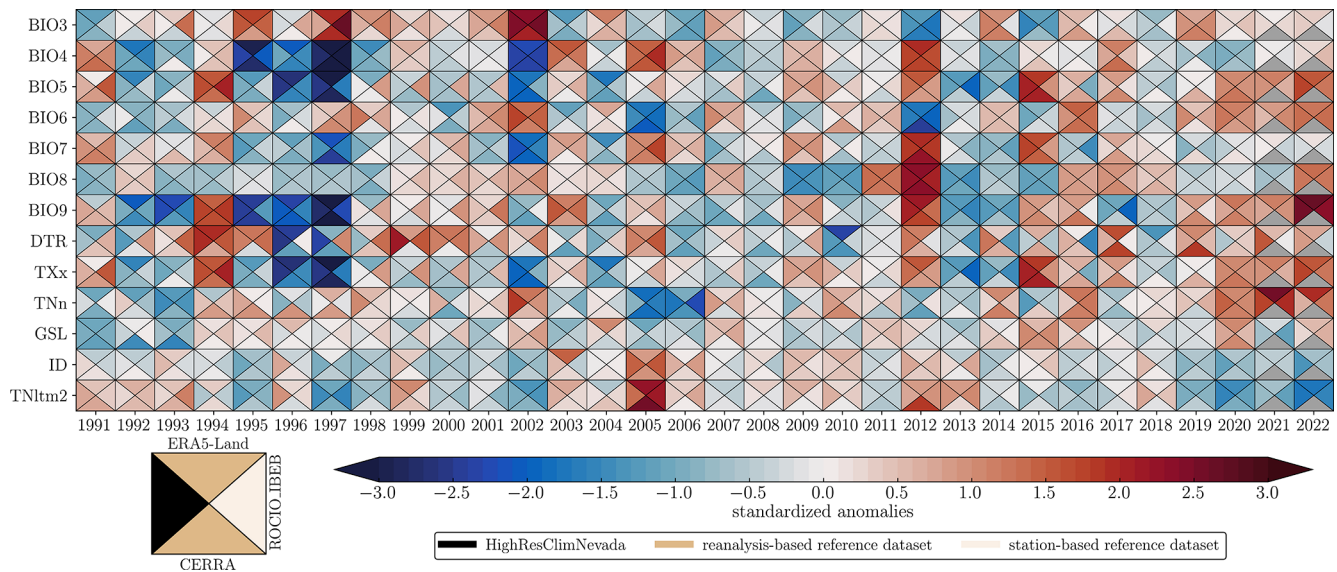
Figure 6. Normalized temperature anomalies for bioclimatic variables and ETCCDI extreme indices. Anomalies are calculated using the mean and standard deviation in a common period (1991–2022) of each database and spatially averaged across the SN Natural Park. Grey triangles indicate that there is no value for that year in the specified database. The legend depicts the sequence of data in each square (in black, HighResClimNevada), with the nature of each database marked by color.

ences the patterns of bioclimatic indices when the precipitation is implicated. This is especially shown in the patterns of the precipitation of the wettest month (BIO13, Fig. 7a) and the precipitation of the coldest quarter (BIO19, Fig. 7c). Moreover, both variables show a very similar spatial pattern, with BIO13 values ranging from 90–350 mm and BIO19 values from 150–750 mm. Precipitation seasonality (BIO15, Fig. 7b), with values ranging from 95 %–120 %, however, appears not to be influenced by orography, showing the lowest values in the north–northwest part of the SN National Park. Extreme ETCCDI indices are also influenced by orography (from Fig. 7d–i). That is, these indices show the highest extreme precipitation at high altitude in the western mountains and the lowest in the outermost natural park's regions. Thus, SN is characterized by R1mm (Fig. 7d), on average, between 35 and 80 rainy days per year, SDII values (Fig. 7g) ranging from 8 and 18 mm d^{-1}, and Rx5d (Fig. 7h) with values between 30 and 140 mm per 5 d. Heavy (R10mm, Fig. 7e) and very heavy (R20mm, Fig. 7f) precipitation days, on the other hand, exhibit similar regional patterns to R1mm, with maximum values exceeding 36 and 26 d yr^{-1}, respectively. In terms of dry spells (CDD, Fig. 7i), HighResClimNevada indicates that the SN Natural Park is affected by 50–120 consecutive dry days. In terms of very extreme precipitation values (from Fig. 7j–l), which are based on hourly precipitation, HighResClimNevada shows that wet hours (hourly pr > 0.1 mm) account for 11 % of the annual hours at the highest peaks, with values falling below 2 % in the southeastern part of the SN National Park (Fig. 7j). The average intensity during wet hours appears to be around

1.6 mm h^{-1} (Fig. 7k), with extreme hourly precipitation of up to 25 mm h^{-1} (Fig. 7l). For these latter indices, the orography has an unclear effect, with the highest values in the west and the south.

When the temporal evolution of precipitation values from HighResClimNevada is compared with other climatic products (Fig. 8), we can note more discrepancies than for temperature in the sign of the anomalies. Such discrepancies are greater when HighResClimNevada is compared to CMORPH, but the latter also disagrees with other climatic products. For example, in 2010, a year characterized by high-precipitation records in the southern part of IP during the winter and spring, strong positive anomalies in BIO19 (i.e., precipitation of the coldest quarter) are depicted except for CMORPH, which indicates normal conditions for that year. Similarly, positive anomalies are observed for BIO13 (i.e., precipitation of the wettest month), but they are lighter than for BIO19. In terms of BIO15 (i.e., precipitation seasonality), however, there is not a clear consensus between datasets for that year. Very extreme precipitation indices indicate that HighResClimNevada performs well according to reference datasets providing hourly data (i.e., GPM IMERG, ERA5-Land, and CMORPH).

4 Code and data availability

Codes, supplementary figure, and HighResClimNevada data are available in García-Valdecasas Ojeda et al. (2025) (https://doi.org/10.5281/zenodo.14883471). At this link, daily values of temperature (mean, maximum, and mini-
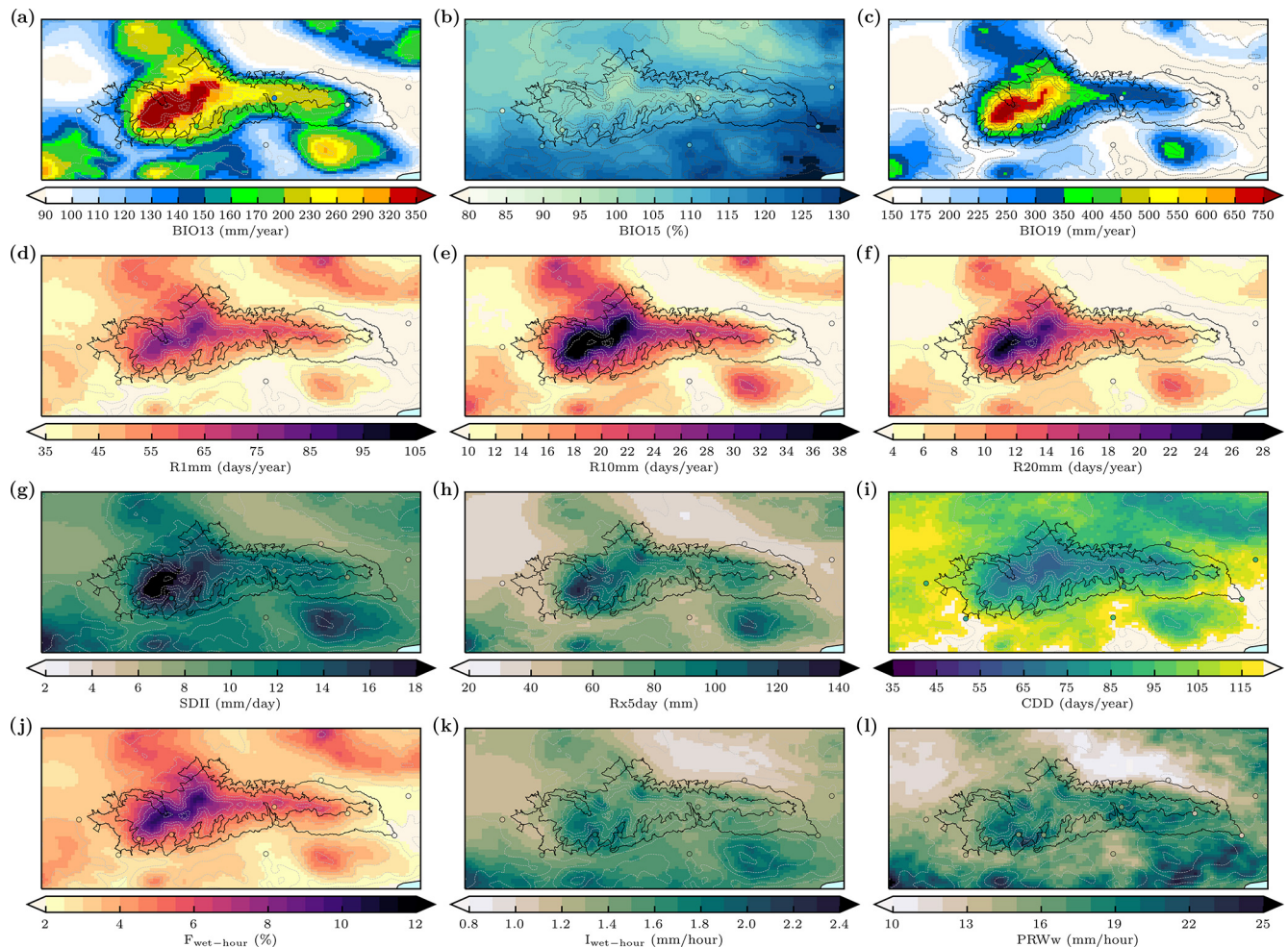
Figure 7. Spatial patterns of bioclimatic variables and extreme ETCCDI indices of precipitation in HighResClimNevada. **(a)** Precipitation of the wettest month (BIO13, $\mathrm{mm\,month^{-1}}$), **(b)** precipitation seasonality (BIO15, $\mathrm{mm\,month^{-1}}$), **(c)** precipitation in the coldest quarter (BIO19, $\mathrm{mm\,month^{-1}}$), **(d)** wet days (R1mm, $\mathrm{d\,yr^{-1}}$), **(e)** heavy precipitation days (R10mm, $\mathrm{d\,yr^{-1}}$), **(f)** very heavy precipitation days (R20mm, $\mathrm{d\,yr^{-1}}$), **(g)** simple daily intensity index (SDII, $\mathrm{mm\,yr^{-1}}$), **(h)** maximum 5 d precipitation (Rx5d, mm), **(i)** consecutive dry days (CDD, $\mathrm{d\,yr^{-1}}$), **(j)** wet-hour frequency ($F_{\mathrm{wet\text{-}day}}$, %), **(k)** wet-hour intensity ($I_{\mathrm{wet\text{-}day}}$, $\mathrm{mm\,h^{-1}}$), and **(l)** maximum amount in the wettest month (PRWw, $\mathrm{mm\,h^{-1}}$). The dots in each panel reflect the values achieved by SAIH stations, while the solid black lines display the national and natural park boundaries.

mum), precipitation, near-surface relative humidity, surface pressure, surface net radiation, and wind speed for the region of Sierra Nevada at 1 km spatial resolution can be found. Additionally, hourly precipitation and temperature datasets are provided as a part of this database as well as bioclimatic variables and extremes. For the evaluation of our HighResClimNevada, different reference data were used, which are all freely available. AEMET 5 km gridded datasets (ROCIO_IBEB version 2) are available online at https://www.aemet.es/es/serviciosclimaticos (last access: January 2024, Peral et al., 2017). UGR-SNGrid is available online on the institutional repository of the Universidad de Granada (https://hdl.handle.net/10481/95487, Romero-Jiménez

et al., 2023). GPM IMERG (https://doi.org/10.5065/7DE2-M746, Huffman et al., 2019) and CMORPH rainfall estimations (https://www.ncei.noaa.gov/data/cmorph-high-resolution-global-precipitation-estimates, Joyce et al., 2004) are freely available online. The Climate Hazards Center of the University of California Santa Barbara provides the CHIRPS data v2 (https://data.chc.ucsb.edu/products/CHIRPS-2.0, Funk et al., 2015) for different domains, formats, and resolutions. Here, the global daily version at 0.05° of spatial resolution was downloaded in netCDF format. CERRA (https://doi.org/10.24381/CDS.A7F3CD0B, Verrelle et al., 2022), CERRA-Land (https://doi.org/10.24381/CDS.622A565A,
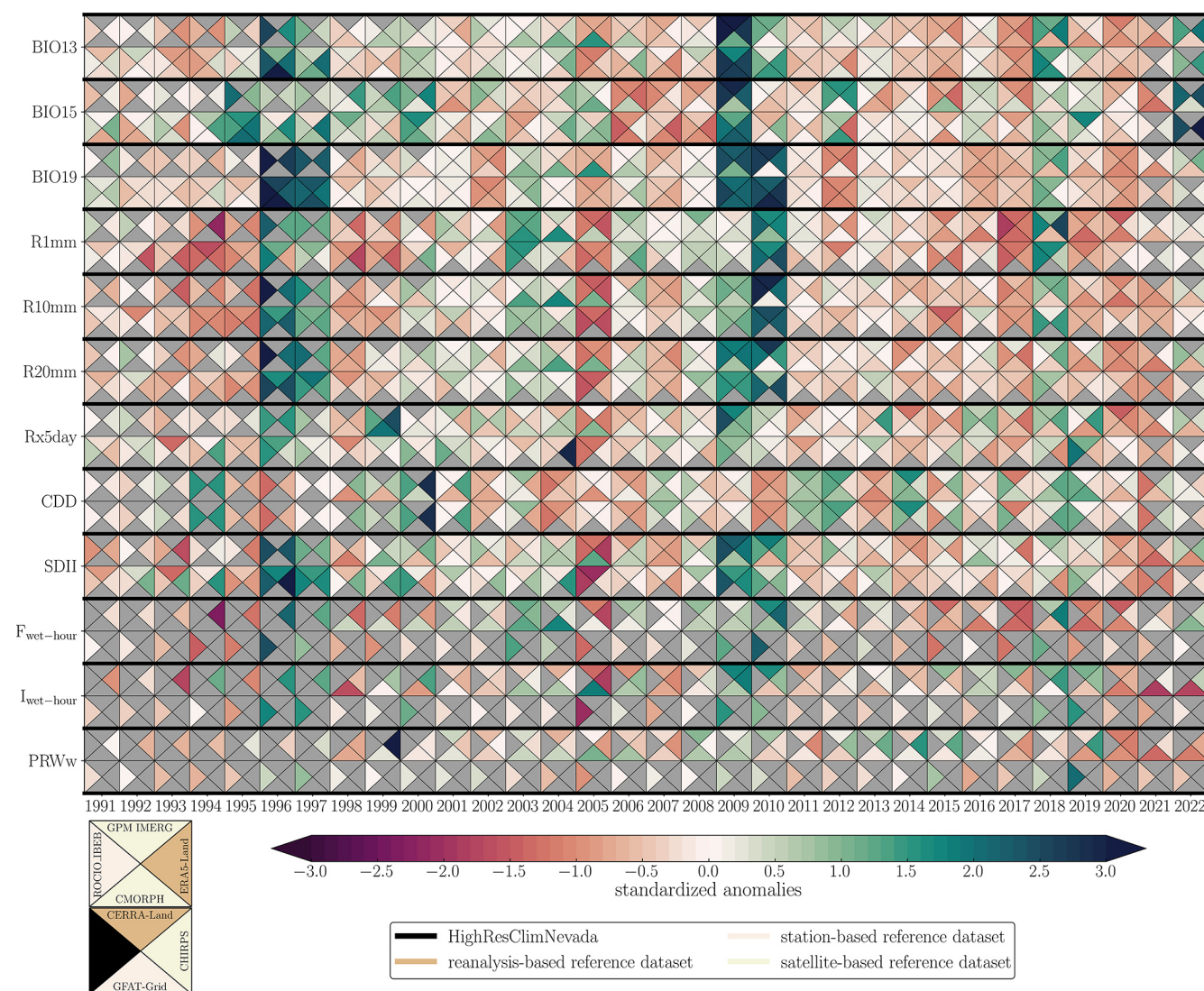
Figure 8. Normalized precipitation anomalies for bioclimatic variables, ETCCDI extreme indices, and precipitation-hour extreme indices. Anomalies are calculated using the mean and standard deviation in a common period (1991–2022) of each database and spatially averaged across the SN Natural Park. Green colors indicate wet anomalies, while red colors show drier-than-normal values. Grey triangles indicate that there is no value for that year in the specified database. The legend depicts the sequence of the data in each square (in black, HighResClimNevada), with the nature of each database marked by colors.

Schimanke et al., 2021), and ERA5-Land (https://doi.org/10.24381/cds.e2161bac, Muñoz-Sabater et al., 2019) are available in the Copernicus Climate Data Store (CDS) (https://cds.climate.copernicus.eu/, last access: 20 September 2023). The weather station data for SN was provided by the SAIH networks, and they are available upon request.

5 Discussion and conclusions

We present HighResClimNevada, a climatological 1 km dataset derived from regional climate modeling. To do that, the Weather Research and Forecasting model v4.3.3 with a

configuration especially designed for Sierra Nevada has been used. SN is a region of special interest due to its high ecological value. Therefore, HighResClimNevada has been developed with the purpose of filling the gap of lack of long-term climate information regular in space and time using climate modeling. This database has been generated based only on climate model outputs and therefore it does not consider information from observations of ground-based stations or satellites via assimilation in order to avoid new sources of uncertainties. Note, observations in this region are usually short and contain errors due to instrumental inaccuracies or poorly calibrated equipment since SN is an area difficult to access. Furthermore, satellite information frequently has substan-

tial uncertainties and short records; hence, assimilation may contribute additional uncertainty into climate data. HighResClimNevada provides hourly and daily primary climate variables structured in netCDF files with variables stored in a 1 km grid from January 1991–December 2022.

Additionally, and due to the special relevance of this region to study the impacts of climate change, bioclimatic variables, extreme ETCCDI climate indices, and hour-precipitation extreme indices derived from hourly precipitation were postprocessed and are also part of this climatic product. HighResClimNevada was compared with reference datasets in order to evaluate its climate performance. These comparisons showed that HighResClimNevada is a valuable tool for assessing trends in temperature variables, in terms of both extreme and mean values, as its performance is similar to that of other products. However, due to its higher resolution, it shows a level of spatial detail, which is physically consistent (due to the nature of the product itself) and necessary for ecological analysis, that is not available in the other products. In terms of precipitation, more discrepancies are shown, although it is important to note the difficulty in obtaining data in this complex region. In fact, it is well known that datasets based on observations often have problems in high-mountain regions due to the challenge of maintaining station networks with an adequate density of stations. Moreover, satellite products like GPM IMERG or CMORPH also show problems characterizing the precipitation amount fallen over mountains, leading to underestimations (Derin and Yilmaz, 2014; Kazamias et al., 2022; Navarro et al., 2020; Tapiador et al., 2020). However, HighResClimNevada shows a similar behavior in many extreme values to reanalysis products such as CERRA-Land and CHIRPS. The HighResClimNevada dataset presented here serves as a scientific basis for assessing the impacts of climate change over SN on many sectors, such as on ecological and hydrological systems.

Author contributions. MGVO: conceptualization, data curation, formal analysis, investigation, methodology, software, validation, visualization, writing (original draft preparation, review, and editing). FSF: data curation, formal analysis, software. DDM: software. ERJ: investigation. JJRC: visualization. YCD: investigation, conceptualization, writing (review and editing), supervision. SRGF: resources, conceptualization, investigation, writing (review and editing), supervision. MJEP: investigation, conceptualization, writing (review and editing), supervision, funding acquisition, project administration.

References

Alzate Velásquez, D. F., Araujo Carrillo, G. A., Rojas Barbosa, E. O., Gomez Latorre, D. A., and Martínez Maldonado, F. E.: Interpolacion Regnie para lluvia y temperatura en las regiones andina, caribe y pacífica de Colombia, Colomb. For., 21, 102, https://doi.org/10.14483/2256201X.11601, 2017.

Argüeso, D., Hidalgo-Muñoz, J. M., Gámiz-Fortis, S. R., Esteban-Parra, M. J., and Castro-Díez, Y.: Evaluation of WRF Mean and Extreme Precipitation over Spain: Present Climate (1970–99), J. Climate, 25, 4883–4897, https://doi.org/10.1175/JCLI-D-11-00276.1, 2012.

Bae, S. Y., Hong, S.-Y., and Tao, W.-K.: Development of a Single-Moment Cloud Microphysics Scheme with Prognostic Hail for the Weather Research and Forecasting (WRF) Model, Asia-Pac. J. Atmos. Sci., 55, 233–245, https://doi.org/10.1007/s13143-018-0066-3, 2019.

Barnard, D. M., Knowles, J. F., Barnard, H. R., Goulden, M. L., Hu, J., Litvak, M. E., and Molotch, N. P.: Reevaluating growing season length controls on net ecosystem production in evergreen conifer forests, Sci. Rep., 8, 17973, https://doi.org/10.1038/s41598-018-36065-0, 2018.

Begert, M. and Frei, C.: Long-term area-mean temperature series for Switzerland – Combining homogenized station data and high resolution grid data, Int. J. Climatol., 38, 2792–2807, https://doi.org/10.1002/joc.5460, 2018.

Beniston, M.: Climatic Change in Mountain Regions: A Review of Possible Impacts, Climatic Change, 59, 5–31, https://doi.org/10.1023/A:1024458411589, 2003.

Beniston, M., Farinotti, D., Stoffel, M., Andreassen, L. M., Coppola, E., Eckert, N., Fantini, A., Giacona, F., Hauck, C., Huss, M., Huwald, H., Lehning, M., López-Moreno, J.-I., Magnusson, J., Marty, C., Morán-Tejéda, E., Morin, S., Naaim, M., Provenzale, A., Rabatel, A., Six, D., Stötter, J., Strasser, U., Terzago, S., and Vincent, C.: The European mountain cryosphere: a review of its current state, trends, and future challenges, The Cryosphere, 12, 759–794, https://doi.org/10.5194/tc-12-759-2018, 2018.

Blanca, G., Cueto, M., Martínez-Lirola, M. J., and Molero-Mesa, J.: Threatened vascular flora of Sierra Nevada (Southern Spain), Biol. Conserv., 85, 269–285, https://doi.org/10.1016/S0006-3207(97)00169-9, 1998.

Collins, W., Rasch, P., Boville, B., McCaa, J., Williamson, D., Kiehl, J., Briegleb, B., Bitz, C., Lin, S.-J., Zhang, M., and Dai, Y.: Description of the NCAR Community Atmosphere Model (CAM 3.0), UCAR/NCAR, https://doi.org/10.5065/D63N21CH, 2004.

Coppola, E., Sobolowski, S., Pichelli, E., Raffaele, F., Ahrens, B., Anders, I., Ban, N., Bastin, S., Belda, M., Belusic, D., Caldas-Alvarez, A., Cardoso, R. M., Davolio, S., Dobler, A., Fernandez, J., Fita, L., Fumiere, Q., Giorgi, F., Goergen, K., Güttler, I., Halenka, T., Heinzeller, D., Hodnebrog, Ø., Jacob, D., Kartsios, S., Katragkou, E., Kendon, E., Khodayar, S., Kunstmann, H., Knist, S., Lavín-Gullón, A., Lind, P., Lorenz, T., Maraun, D., Marelle, L., Van Meijgaard, E., Milovac, J., Myhre, G., Panitz, H.-J., Piazza, M., Raffa, M., Raub, T., Rockel, B., Schär, C., Sieck, K., Soares, P. M. M., Somot, S., Srnec, L., Stocchi, P., Tölle, M. H., Truhetz, H., Vautard, R., De Vries, H., and Warrach-Sagi, K.: A first-of-its-kind multi-model convection permitting ensemble for investigating convective phenomena over Europe and the Mediterranean, Clim. Dynam., 55, 3–34, https://doi.org/10.1007/s00382-018-4521-8, 2020.

Denis, B., Laprise, R., and Caya, D.: Sensitivity of a regional climate model to the resolution of the lateral boundary conditions, Clim. Dynam., 20, 107–126, https://doi.org/10.1007/s00382-002-0264-6, 2003.

Derin, Y. and Yilmaz, K. K.: Evaluation of Multiple Satellite-Based Precipitation Products over Complex Topography, J. Hydrometeorol., 15, 1498–1516, https://doi.org/10.1175/JHM-D-13-0191.1, 2014.

Esteban-Parra, M. J., García-Valdecasas Ojeda, M., Peinó-Calero, E., Romero-Jiménez, E., Yeste, P., Rosa-Cánovas, J. J., Rodríguez-Brito, A., Gámiz-Fortis, S. R., and Castro-Díez, Y.: Climate Variability and Trends, in: The Landscape of the Sierra Nevada, edited by: Zamora, R. and Oliva, M., Springer International Publishing, Cham, 129–148, https://doi.org/10.1007/978-3-030-94219-9_9, 2022.

Fick, S. E. and Hijmans, R. J.: WorldClim 2: new 1 km spatial resolution climate surfaces for global land areas, Int. J. Climatol., 37, 4302–4315, https://doi.org/10.1002/joc.5086, 2017.

Frich, P., Alexander, L., Della-Marta, P., Gleason, B., Haylock, M., Klein Tank, A., and Peterson, T.: Observed coherent changes in climatic extremes during the second half of the twentieth century, Clim. Res., 19, 193–212, https://doi.org/10.3354/cr019193, 2002.

Funk, C., Peterson, P., Landsfeld, M., Pedreros, D., Verdin, J., Shukla, S., Husak, G., Rowland, J., Harrison, L., Hoell, A., and Michaelsen, J.: The climate hazards infrared precipitation with stations – a new environmental record for monitoring extremes, Sci. Data, 2, 150066, https://doi.org/10.1038/sdata.2015.66,

2015 (data available at: https://data.chc.ucsb.edu/products/CHIRPS-2.0, last access: 20 September 2023).

Garcia-Valdecasas Ojeda, M., Solano Farías, F., Donaire Montaño, D., Romero-Jiménez, E., Rosa-Cánovas, J. J., Gámiz-Fortis, S. R., Castro-Díez, Y., and Esteban-Parra, M. J.: HighResClimNevada: a high-resolution climatological dataset for a high-altitude region in Southern Spain (Sierra Nevada), Zenodo [code and data set], https://doi.org/10.5281/ZENODO.14883471, 2025.

Gobiet, A., Kotlarski, S., Beniston, M., Heinrich, G., Rajczak, J., and Stoffel, M.: 21st century climate change in the European Alps – A review, Sci. Total Environ., 493, 1138–1151, https://doi.org/10.1016/j.scitotenv.2013.07.050, 2014.

González-Rojí, S. J., Messmer, M., Raible, C. C., and Stocker, T. F.: Sensitivity of precipitation in the highlands and lowlands of Peru to physics parameterization options in WRFV3.8.1, Geosci. Model Dev., 15, 2859–2879, https://doi.org/10.5194/gmd-15-2859-2022, 2022.

Grell, G. A. and Freitas, S. R.: A scale and aerosol aware stochastic convective parameterization for weather and air quality modeling, Atmos. Chem. Phys., 14, 5233–5250, https://doi.org/10.5194/acp-14-5233-2014, 2014.

Halladay, K., Berthou, S., and Kendon, E.: Improving land surface feedbacks to the atmosphere in convection-permitting climate simulations for Europe, Clim. Dynam., https://doi.org/10.1007/s00382-024-07192-4, 2024.

Hartmann, D. L., Wallace, J. M., Limpasuvan, V., Thompson, D. W. J., and Holton, J. R.: Can ozone depletion and global warming interact to produce rapid climate change?, P. Natl. Acad. Sci. USA, 97, 1412–1417, https://doi.org/10.1073/pnas.97.4.1412, 2000.

Hersbach, H., Bell, B., Berrisford, P., Hirahara, S., Horányi, A., Muñoz-Sabater, J., Nicolas, J., Peubey, C., Radu, R., Schepers, D., Simmons, A., Soci, C., Abdalla, S., Abellan, X., Balsamo, G., Bechtold, P., Biavati, G., Bidlot, J., Bonavita, M., De Chiara, G., Dahlgren, P., Dee, D., Diamantakis, M., Dragani, R., Flemming, J., Forbes, R., Fuentes, M., Geer, A., Haimberger, L., Healy, S., Hogan, R. J., Hólm, E., Janisková, M., Keeley, S., Laloyaux, P., Lopez, P., Lupu, C., Radnoti, G., De Rosnay, P., Rozum, I., Vamborg, F., Villaume, S., and Thépaut, J.: The ERA5 global reanalysis, Q. J. R. Meteor. Soc., 146, 1999–2049, https://doi.org/10.1002/qj.3803, 2020.

Hersbach, H., Bell, B., Berrisford, P., Biavati, G., Horányi, A., Muñoz Sabater, J., Nicolas, J., Peubey, C., Radu, R., Rozum, I., Schepers, D., Simmons, A., Soci, C., Dee, D., and Thépaut, J.-N.: ERA5 hourly data on single levels from 1940 to present, Copernicus Climate Change Service (C3S) Climate Data Store (CDS) [data set], https://doi.org/10.24381/cds.adbb2d47, 2023.

Hijmans, R. J., Cameron, S. E., Parra, J. L., Jones, P. G., and Jarvis, A.: Very high resolution interpolated climate surfaces for global land areas, Int. J. Climatol., 25, 1965–1978, https://doi.org/10.1002/joc.1276, 2005.

Huffman, G. J., Stocker, E. F., Bolvin, D. T., Nelkin, E. J., and Jackson, T.: GPM IMERG Final Precipitation L3 1 day 0.1 degree x 0.1 degree V07, NSF [data set], https://doi.org/10.5065/7DE2-M746, 2019.

Huffman, G. J., Bolvin, D. T., Braithwaite, D., Hsu, K.-L., Joyce, R. J., Kidd, C., Nelkin, E. J., Sorooshian, S., Stocker, E. F., Tan, J., Wolff, D. B., and Xie, P.: Integrated Multi-satellite Re-

trievals for the Global Precipitation Measurement (GPM) Mission (IMERG), in: Satellite Precipitation Measurement, vol. 67, edited by: Levizzani, V., Kidd, C., Kirschbaum, D. B., Kummerow, C. D., Nakamura, K., and Turk, F. J., Springer International Publishing, Cham, 343–353, https://doi.org/10.1007/978-3-030-24568-9_19, 2020.

Jerez, S., López-Romero, J. M., Turco, M., Lorente-Plazas, R., Gómez-Navarro, J. J., Jiménez-Guerrero, P., and Montávez, J. P.: On the Spin-Up Period in WRF Simulations Over Europe: Trade-Offs Between Length and Seasonality, J. Adv. Model. Earth Sy., 12, e2019MS001945, https://doi.org/10.1029/2019MS001945, 2020.

Jiménez, P. A., Dudhia, J., González-Rouco, J. F., Navarro, J., Montávez, J. P., and García-Bustamante, E.: A Revised Scheme for the WRF Surface Layer Formulation, Mon. Weather Rev., 140, 898–918, https://doi.org/10.1175/MWR-D-11-00056.1, 2012.

Joyce, R. J., Janowiak, J. E., Arkin, P. A., and Xie, P.: CMORPH: A Method that Produces Global Precipitation Estimates from Passive Microwave and Infrared Data at High Spatial and Temporal Resolution, J. Hydrometeorol., 5, 487–503, https://doi.org/10.1175/1525-7541(2004)005<0487:CAMTPG>2.0.CO;2, 2004 (data available at: https://www.ncei.noaa.gov/data/cmorph-high-resolution-global-precipitation-estimates, last access: January 2024).

Karger, D. N., Conrad, O., Böhner, J., Kawohl, T., Kreft, H., Soria-Auza, R. W., Zimmermann, N. E., Linder, H. P., and Kessler, M.: Climatologies at high resolution for the earth's land surface areas, Sci. Data, 4, 170122, https://doi.org/10.1038/sdata.2017.122, 2017.

Kazamias, A.-P., Sapountzis, M., and Lagouvardos, K.: Evaluation of GPM-IMERG rainfall estimates at multiple temporal and spatial scales over Greece, Atmos. Res., 269, 106014, https://doi.org/10.1016/j.atmosres.2021.106014, 2022.

Khodayar, S., Sehlinger, A., Feldmann, H., and Kottmeier, C.: Sensitivity of soil moisture initialization for decadal predictions under different regional climatic conditions in Europe, Int. J. Climatol., 35, 1899–1915, https://doi.org/10.1002/joc.4096, 2015.

La Sorte, F. A. and Jetz, W.: Projected range contractions of montane biodiversity under global warming, P. R. Soc. B., 277, 3401–3410, https://doi.org/10.1098/rspb.2010.0612, 2010.

Liu, Q., Piao, S., Janssens, I. A., Fu, Y., Peng, S., Lian, X., Ciais, P., Myneni, R. B., Peñuelas, J., and Wang, T.: Extension of the growing season increases vegetation exposure to frost, Nat. Commun., 9, 426, https://doi.org/10.1038/s41467-017-02690-y, 2018.

Lucas-Picher, P., Brisson, E., Caillaud, C., Alias, A., Nabat, P., Lemonsu, A., Poncet, N., Cortés Hernandez, V. E., Michau, Y., Doury, A., Monteiro, D., and Somot, S.: Evaluation of the convection-permitting regional climate model CNRM-AROME41t1 over Northwestern Europe, Clim. Dynam., 62, 4587–4615, https://doi.org/10.1007/s00382-022-06637-y, 2024.

Matte, D., Laprise, R., and Thériault, J. M.: Comparison between high-resolution climate simulations using single- and double-nesting approaches within the Big-Brother experimental protocol, Clim. Dynam., 47, 3613–3626, https://doi.org/10.1007/s00382-016-3031-9, 2016.

Messmer, M., González-Rojí, S. J., Raible, C. C., and Stocker, T. F.: Sensitivity of precipitation and temperature over the Mount Kenya area to physics parameterization

options in a high-resolution model simulation performed with WRFV3.8.1, Geosci. Model Dev., 14, 2691–2711, https://doi.org/10.5194/gmd-14-2691-2021, 2021.

Muñoz Sabater, J.: ERA5-Land hourly data from 1950 to present, Copernicus Climate Change Service (C3S) Climate Data Store (CDS) [data set], https://doi.org/10.24381/cds.e2161bac, 2019.

Muñoz-Sabater, J., Dutra, E., Agustí-Panareda, A., Albergel, C., Arduini, G., Balsamo, G., Boussetta, S., Choulga, M., Harrigan, S., Hersbach, H., Martens, B., Miralles, D. G., Piles, M., Rodríguez-Fernández, N. J., Zsoter, E., Buontempo, C., and Thépaut, J.-N.: ERA5-Land: a state-of-the-art global reanalysis dataset for land applications, Earth Syst. Sci. Data, 13, 4349–4383, https://doi.org/10.5194/essd-13-4349-2021, 2021.

Navarro, A., García-Ortega, E., Merino, A., Sánchez, J. L., and Tapiador, F. J.: Orographic biases in IMERG precipitation estimates in the Ebro River basin (Spain): The effects of rain gauge density and altitude, Atmos. Res., 244, 105068, https://doi.org/10.1016/j.atmosres.2020.105068, 2020.

Nigrelli, G. and Chiarle, M.: 1991–2020 climate normal in the European Alps: focus on high-elevation environments, J. Mt. Sci., 20, 2149–2163, https://doi.org/10.1007/s11629-023-7951-7, 2023.

Noce, S., Caporaso, L., and Santini, M.: A new global dataset of bioclimatic indicators, Sci. Data, 7, 398, https://doi.org/10.1038/s41597-020-00726-5, 2020.

O'Donnell, M. S. and Ignizio, D. A.: Bioclimatic Predictors for Supporting Ecological Applications in the Conterminous United States, Data Series No. 691, U.S. Geological Survey, 1–10, https://doi.org/10.3133/ds691, 2012.

Oliva, M., Fernández-Fernández, J. M., and Martín-Díaz, J.: The Geographic Uniqueness of the Sierra Nevada in the Context of the Mid-Latitude Mountains, in: The Landscape of the Sierra Nevada, edited by: Zamora, R. and Oliva, M., Springer International Publishing, Cham, 3–9, https://doi.org/10.1007/978-3-030-94219-9_1, 2022.

Parmesan, C.: Ecological and Evolutionary Responses to Recent Climate Change, Annu. Rev. Ecol. Evol. S., 37, 637–669, https://doi.org/10.1146/annurev.ecolsys.37.091305.110100, 2006.

Pepin, N., Deng, H., Zhang, H., Zhang, F., Kang, S., and Yao, T.: An Examination of Temperature Trends at High Elevations Across the Tibetan Plateau: The Use of MODIS LST to Understand Patterns of Elevation-Dependent Warming, JGR Atmospheres, 124, 5738–5756, https://doi.org/10.1029/2018JD029798, 2019.

Pepin, N. C., Arnone, E., Gobiet, A., Haslinger, K., Kotlarski, S., Notarnicola, C., Palazzi, E., Seibert, P., Serafin, S., Schöner, W., Terzago, S., Thornton, J. M., Vuille, M., and Adler, C.: Climate Changes and Their Elevational Patterns in the Mountains of the World, Rev. Geophys., 60, e2020RG000730, https://doi.org/10.1029/2020RG000730, 2022.

Peral García, C., Navascués Fernández-Victorio, B., and Ramos Calzado, P.: Serie de precipitación diaria en rejilla con fines climáticos, Agencia Estatal de Meteorología, https://doi.org/10.31978/014-17-009-5, 2017.

Pleim, J. E.: A Combined Local and Nonlocal Closure Model for the Atmospheric Boundary Layer. Part I: Model Description and Testing, J. Appl. Meteorol. Clim., 46, 1383–1395, https://doi.org/10.1175/JAM2539.1, 2007.

Polo, M. J., Herrero, J., Pimentel, R., and Pérez-Palazón, M. J.: The Guadalfeo Monitoring Network (Sierra Nevada, Spain): 14 years

of measurements to understand the complexity of snow dynamics in semiarid regions, Earth Syst. Sci. Data, 11, 393–407, https://doi.org/10.5194/essd-11-393-2019, 2019.

Polo, M. J., Pimentel, R., Gascoin, S., and Notarnicola, C.: Mountain hydrology in the Mediterranean region, in: Water Resources in the Mediterranean Region, edited by: Zribi, M., Brocca, L., Tramblay, Y., and Molle, F., Elsevier, 51–75, https://doi.org/10.1016/B978-0-12-818086-0.00003-0, 2020.

Pleim, J. E.: A Combined Local and Nonlocal Closure Model for the Atmospheric Boundary Layer. Part II: Application and Evaluation in a Mesoscale Meteorological Model, J. Appl. Meteorol. Clim., 46, 1396–1409, https://doi.org/10.1175/JAM2534.1, 2007.

Prein, A. F. and Gobiet, A.: Impacts of uncertainties in European gridded precipitation observations on regional climate analysis, Int. J. Climatol., 37, 305–327, https://doi.org/10.1002/joc.4706, 2017.

Prein, A. F., Langhans, W., Fosser, G., Ferrone, A., Ban, N., Goergen, K., Keller, M., Tölle, M., Gutjahr, O., Feser, F., Brisson, E., Kollet, S., Schmidli, J., Van Lipzig, N. P. M., and Leung, R.: A review on regional convection-permitting climate modeling: Demonstrations, prospects, and challenges, Rev. Geophys., 53, 323–361, https://doi.org/10.1002/2014RG000475, 2015.

Prein, A. F., Rasmussen, R., and Stephens, G.: Challenges and Advances in Convection-Permitting Climate Modeling, B. Am. Meteorol. Soc., 98, 1027–1030, https://doi.org/10.1175/BAMS-D-16-0263.1, 2017.

Prein, A. F., Rasmussen, R., Castro, C. L., Dai, A., and Minder, J.: Special issue: Advances in convection-permitting climate modeling, Clim. Dynam., 55, 1–2, https://doi.org/10.1007/s00382-020-05240-3, 2020.

Rangwala, I. and Miller, J. R.: Climate change in mountains: a review of elevation-dependent warming and its possible causes, Climatic Change, 114, 527–547, https://doi.org/10.1007/s10584-012-0419-3, 2012.

Rauthe, M., Steiner, H., Riediger, U., Mazurkiewicz, A., and Gratzki, A.: A Central European precipitation climatology Part I: Generation and validation of a high-resolution gridded daily data set (HYRAS), metz, 22, 235–256, https://doi.org/10.1127/0941-2948/2013/0436, 2013.

Romero-Jiménez, E., Cepeda-Ventura, L., García-Valdecasas Ojeda, M., Rosa-Cánovas, J. J., Romero-Jiménez, E., Cepeda-Ventura, L., García-Valdecasas Ojeda, M., Rosa-Cánovas, J. J., Donaire-Montaño, D., Solano-Farías, F., Toro Ortiz, Y., Gámiz-Fortis, S. R., Castro-Díez, Y., and Esteban-Parra, M. J.: Creating a gridded climate database in Sierra Nevada, in the southern Iberian Peninsula, EMS Annual Meeting 2023, Bratislava, Slovakia, 4–8 Sep 2023, EMS2023-463, https://doi.org/10.5194/ems2023-463, 2023.

Romero-Jiménez, E., Cepeda-Ventura, L., García-Valdecasas Ojeda, M., Rosa-Cánovas, J. J., Castro-Díez, Y., Gámiz-Fortis, S. R., and Esteban-Parra, M. J.: UGR-SNGrid: Datos de Precipitación Mensual para Sierra Nevada, Zenodo [data set], https://doi.org/10.5281/ZENODO.13885000, 2024.

Sangelantoni, L., Sobolowski, S., Lorenz, T., Hodnebrog, Ø., Cardoso, R. M. C., Soares, P., Ferretti, R., Lavín-Gullón, A., Fernandez, J., Goergen, K., Milovac, J., Katragkou, E., Kartsios, S., Coppola, E., Pichelli, E., Adinolfi, M., Mercogliano, P., Berthou, S., De Vries, H., Dobler, A., Belušić, D., Feldmann, H.,

Tölle, M., and Bastin, S.: Investigating the Representation of Heatwaves from an Ensemble of km-scale Regional Climate Simulations within CORDEX-FPS Convection, Research Square [preprint], https://doi.org/10.21203/rs.3.rs-1395524/v1, 2 March 2022.

Schimanke, S., Ridal, M., Le Moigne, P., Berggren, L., Undén, P., Randriamampianina, R., Andrea, U., Bazile, E., Bertelsen, A., Brousseau, P., Dahlgren, P., Edvinsson, L., El Said, A., Glinton, M., Hopsch, S., Isaksson, L., Mladek, R., Olsson, E., Verrelle, A., and Wang, Z. Q.: CERRA sub-daily regional reanalysis data for Europe on single levels from 1984 to present, Copernicus Climate Change Service (C3S) Climate Data Store (CDS) [data set], https://doi.org/10.24381/CDS.622A565A, 2021.

Sigro, J., Cisneros, M., Perez-Luque, A. J., Perez-Martinez, C., and Vegas-Vilarrubia, T.: Trends in temperature and precipitation at high and low elevations in the main mountain ranges of the Iberian Peninsula (1894–2020): The Sierra Nevada and the Pyrenees, Int. J. Climatol., 44, 2897–2920, https://doi.org/10.1002/joc.8487, 2024.

Skamarock, W. C., Klemp, J. B., Dudhia, J., Gill, D. O., Liu, Z., Berner, J., Wang, W., Powers, J. G., Duda, M. G., Barker, D. M., and Huang, X.-Y.: A Description of the Advanced Research WRF Model Version 4.3, UCAR/NCAR, https://doi.org/10.5065/1DFH-6P97, 2021.

Solano-Farias, F., García-Valdecasas Ojeda, M., Donaire-Montaño, D., Rosa-Cánovas, J. J., Castro-Díez, Y., Esteban-Parra, M. J., and Gámiz-Fortis, S. R.: Assessment of physical schemes for WRF model in convection-permitting mode over southern Iberian Peninsula, Atmos. Res., 299, 107175, https://doi.org/10.1016/j.atmosres.2023.107175, 2024.

Tapiador, F. J., Navarro, A., García-Ortega, E., Merino, A., Sánchez, J. L., Marcos, C., and Kummerow, C.: The Contribution of Rain Gauges in the Calibration of the IMERG Product: Results from the First Validation over Spain, J. Hydrometeorol., 21, 161–182, https://doi.org/10.1175/JHM-D-19-0116.1, 2020.

Verrelle, A., Glinton, M., Bazile, E., Le Moigne, P., Randriamampianina, R., Ridal, M., Berggren, L., Undén, P., Schimanke, S., Mladek, R., and Soci, C.: CERRA-Land sub-daily regional reanalysis data for Europe from 1984 to present, Copernicus Climate Change Service (C3S) Climate Data Store (CDS) [data set], https://doi.org/10.24381/CDS.A7F3CD0B, 2022.

Viterbi, R., Cerrato, C., Bassano, B., Bionda, R., Hardenberg, A., Provenzale, A., and Bogliani, G.: Patterns of biodiversity in the northwestern Italian Alps: a multi-taxa approach, Community Ecol., 14, 18–30, https://doi.org/10.1556/ComEc.14.2013.1.3, 2013.

Viviroli, D., Kummu, M., Meybeck, M., Kallio, M., and Wada, Y.: Increasing dependence of lowland populations on mountain water resources, Nat. Sustain., 3, 917–928, https://doi.org/10.1038/s41893-020-0559-9, 2020.

Yang, Z.-L., Niu, G.-Y., Mitchell, K. E., Chen, F., Ek, M. B., Barlage, M., Longuevergne, L., Manning, K., Niyogi, D., Tewari, M., and Xia, Y.: The community Noah land surface model with multiparameterization options (Noah-MP): 2. Evaluation over global river basins, J. Geophys. Res., 116, D12110, https://doi.org/10.1029/2010JD015140, 2011.